



CERN-EP-2018-267
 LHCb-PAPER-2018-035
 January 29, 2020

Study of Υ production in $p\text{Pb}$ collisions at $\sqrt{s_{\text{NN}}} = 8.16 \text{ TeV}$

LHCb collaboration[†]

Abstract

The production of $\Upsilon(nS)$ mesons ($n = 1, 2, 3$) in $p\text{Pb}$ and $\text{Pb}p$ collisions at a centre-of-mass energy per nucleon pair $\sqrt{s_{\text{NN}}} = 8.16 \text{ TeV}$ is measured by the LHCb experiment, using a data sample corresponding to an integrated luminosity of 31.8 nb^{-1} . The $\Upsilon(nS)$ mesons are reconstructed through their decays into two opposite-sign muons. The measurements comprise the differential production cross-sections of the $\Upsilon(1S)$ and $\Upsilon(2S)$ states, their forward-to-backward ratios and nuclear modification factors, performed as a function of the transverse momentum p_{T} and rapidity in the nucleon-nucleon centre-of-mass frame y^* of the $\Upsilon(nS)$ states, in the kinematic range $p_{\text{T}} < 25 \text{ GeV}/c$ and $1.5 < y^* < 4.0$ ($-5.0 < y^* < -2.5$) for $p\text{Pb}$ ($\text{Pb}p$) collisions. In addition, production cross-sections for $\Upsilon(3S)$ are measured integrated over phase space and the production ratios between all three $\Upsilon(nS)$ states are determined. The measurements are compared to theoretical predictions and suppressions for quarkonium in $p\text{Pb}$ collisions are observed.

Submitted to JHEP

© 2020 CERN for the benefit of the LHCb collaboration. CC-BY-4.0 licence.

[†]Authors are listed at the end of this paper.

1 Introduction

Existing experimental results in collisions of ultra-relativistic heavy nuclei are consistent with the formation of a deconfined state of hot partonic matter, referred to as Quark-Gluon Plasma (QGP) [1, 2]. One of the signatures of QGP is the suppression of heavy-quarkonia production in the collisions of heavy nuclei (AA collisions) with respect to pp collisions, an effect that is enhanced for states with lower binding energies, such as the $\Upsilon(3S)$ meson [3]. However, the suppression of heavy-quarkonia production can also occur in the collisions of protons with heavy nuclei (pA collisions), where traditionally it was assumed that there was no QGP created.

In pA collisions, this suppression is caused by nuclear phenomena unrelated to deconfinement, commonly called cold nuclear matter (CNM) effects. The CNM effects that are expected to affect quarkonia production are of two types, “initial-state” effects happening at an early stage of the collision, such as nuclear effects on parton densities [4–7] or coherent energy losses [8–10], and “final-state” effects, as quarkonia absorption by nucleons [11], expected to be negligible at LHC energies [12–15]. Another final-state effect is the breaking of the $q\bar{q}$ pair caused by collisions with comoving particles with similar rapidities (the so-called “comovers” model [16–20]), whose density is determined from the particle multiplicity measured in that region of rapidity. This model could explain the relative suppression observed among the $\Upsilon(nS)$ states both in PbPb [21] and in pA collisions [22]. The size of nuclear effects can be quantified by measuring the nuclear modification factor R_{pA} , which is defined as the ratio of the cross-section in pA collisions to that in pp collisions scaled by the number of nucleons in the nucleus. In the absence of modifications, R_{pA} is unity.

Previous measurements in AA collisions at RHIC [23] and LHC [22, 24–27] have revealed sizable nuclear modification factors for the $\Upsilon(nS)$ states which increase with n . Using a data sample corresponding to an integrated luminosity of about 1.5 nb^{-1} , the LHCb collaboration measured [28] the production of $\Upsilon(nS)$ mesons in $p\text{Pb}$ collisions at a per-nucleon centre-of-mass energy of $\sqrt{s_{\text{NN}}} = 5 \text{ TeV}$. Moreover, the measurement of nuclear modification and forward-backward production ratios for $\Upsilon(1S)$, as well as $\Upsilon(nS)$ to $\Upsilon(1S)$ ratios were performed.

In this paper, the production of $\Upsilon(nS)$ mesons is studied in $p\text{Pb}$ collisions using data collected at $\sqrt{s_{\text{NN}}} = 8.16 \text{ TeV}$ with the LHCb detector, corresponding to a total integrated luminosity of 31.8 nb^{-1} . This dataset has been used already for the study of the production of prompt J/ψ and J/ψ coming from b -hadron decays (called nonprompt J/ψ in the following) [29]. The measurements presented here comprise the differential production cross-sections of the $\Upsilon(1S)$ and $\Upsilon(2S)$ states, their forward-to-backward ratios and nuclear modification factors, and the production ratios between all three $\Upsilon(nS)$ states. In addition, the ratio of $\Upsilon(1S)$ to nonprompt J/ψ cross-sections is determined as a function of proton-nucleon centre-of-mass rapidity, y^* , integrated over the transverse momenta, p_T , of the mesons, a measurement that allows direct comparison of open heavy-flavour and quarkonia production in the environment of heavy-nuclei collisions.

2 Detector description and data samples

The LHCb detector [30, 31] is a single-arm forward spectrometer designed for the study of particles containing b or c quarks. The detector includes a high-precision tracking system consisting of a silicon-strip vertex detector surrounding the beam-beam interaction region [32], a large-area silicon-strip detector located upstream of a dipole magnet with a bending power of about 4 Tm, and three stations of silicon-strip detectors and straw drift tubes [33] placed downstream of the magnet. The tracking system provides a measurement of the momentum of charged particles with a relative uncertainty that varies from 0.5% at low momentum to 1.0% at 200 GeV/ c . The minimum distance of a track to a collision vertex, the impact parameter, is measured with a resolution of $(15 + 29/p_T)$ μm , where p_T is in GeV/ c . Different types of charged hadrons are distinguished using information from two ring-imaging Cherenkov detectors [34]. Photons, electrons and hadrons are identified by a calorimeter system consisting of scintillating-pad and preshower detectors, an electromagnetic calorimeter and a hadronic calorimeter. Muons are identified by a system composed of alternating layers of iron and multiwire proportional chambers [35].

The trigger [36] consists of a hardware stage, based on information from the calorimeter and muon systems, followed by a software stage, in which all charged particles with $p_T > 300$ MeV/ c are reconstructed. The alignment and calibration of the detector is performed in near real-time [37]. This alignment is also used later in the offline reconstruction, ensuring consistent and high-quality particle identification (PID) information in the online and offline processing. The identical performance of the online and offline reconstruction offers the opportunity to perform physics analyses directly using candidates reconstructed in the trigger [36, 38] as well as storing information about all reconstructed particles in the event [39]. The storage of only the triggered candidates enables a reduction of the event size by an order of magnitude.

For this analysis, at least one muon with $p_T > 500$ MeV/ c is required at the hardware trigger stage and at the software trigger stage, two muon tracks with $p_T > 300$ MeV/ c and a high-quality reconstructed decay vertex are required to form an $\Upsilon(nS)$ candidate with invariant mass $m(\mu^+\mu^-) > 4.7$ GeV/ c^2 . In addition, a small fraction of events with a large number of tracks in the vertex detector are rejected.

Simulation is used in the determination of efficiencies. The $p\text{Pb}$ collisions are simulated with EPOS-LHC [40] and the $\Upsilon(nS) \rightarrow \mu^+\mu^-$ decays with PYTHIA 8.1 [41] in pp collisions where the proton energy is equal to that in $p\text{Pb}$ collisions. The interaction of the generated particles with the detector and its response are implemented using the GEANT4 toolkit [42], as described in Ref. [43]. The $\Upsilon(nS)$ mesons are produced unpolarised, justified by the fact that the polarisation of $\Upsilon(nS)$ mesons has been measured by LHCb in pp collisions at similar energies and found to be small [44]. Consistently with what was done in previous LHCb analyses [29], no systematic uncertainty is associated with this assumption.

The asymmetric layout of the LHCb experiment [30], which covers the pseudorapidity range of $2 < \eta < 5$, results in two configurations: in the *forward pPb (backward Pb p)* configuration, the proton (lead) beam travels from the VELO detector to the muon chambers, taking advantage of the inversion of the proton and lead beams during the $p\text{Pb}$ data-taking run. The energy of the proton beam is 6.5 TeV, while that of the lead beam is 2.56 TeV per nucleon, resulting in a centre-of-mass energy of the proton-nucleon system of 8.16 TeV. Since the energy per nucleon in the proton beam is significantly larger than that in the lead beam, the proton-nucleon centre-of-mass system has a rapidity in the laboratory

frame of +0.465 (−0.465) for $p\text{Pb}$ (Pbp) collisions, resulting in a shift of the range of the centre-of-mass rapidity y^* in the proton nucleus case. In this analysis, $\Upsilon(nS)$ mesons are measured in the kinematic range of $p_{\text{T}} < 25 \text{ GeV}/c$, and $1.5 < y^* < 4.0$ for $p\text{Pb}$ forward and $-5.0 < y^* < -2.5$ for $p\text{Pb}$ backward collisions. This is the first measurement of $\Upsilon(3S)$ production in $p\text{Pb}$ collisions in this kinematic range. The data samples correspond to an integrated luminosity of $12.5 \pm 0.3 \text{ nb}^{-1}$ in the forward configuration and $19.3 \pm 0.5 \text{ nb}^{-1}$ in the backward configuration. The luminosities are determined using van der Meer scans [45], which were performed for both beam configurations.

3 Definition of the observables

The observables are measured in bins of p_{T} and y^* of the $\Upsilon(1S)$ and $\Upsilon(2S)$ mesons, where both p_{T} and y^* are defined with respect to the direction of the proton beam in the centre-of-mass frame. For the $\Upsilon(3S)$ meson, due to the limited signal yield, only integrated observables are measured.

The differential cross-section is measured in a fixed bin size of 0.5 units for y^* and variable bin sizes for p_{T} in the $0\text{--}25 \text{ GeV}/c$ range. The $\Upsilon(nS)$ meson double-differential production cross-section in the proton-lead collisions is defined as

$$\frac{d^2\sigma}{dp_{\text{T}}dy^*} = \frac{N(\Upsilon(nS) \rightarrow \mu^+\mu^-)}{\mathcal{L} \times \varepsilon_{\text{tot}}^{\Upsilon(nS)} \times \mathcal{B}_{\mu\mu}^{\Upsilon(nS)} \times \Delta p_{\text{T}} \times \Delta y^*}, \quad (1)$$

where $N(\Upsilon(nS) \rightarrow \mu^+\mu^-)$ is the raw yield of the $\Upsilon(nS)$ decays reconstructed in the given rapidity and transverse momentum bin, $\varepsilon_{\text{tot}}^{\Upsilon(nS)}$ is the total efficiency in that bin, including acceptance, $\mathcal{B}_{\mu\mu}^{\Upsilon(nS)}$ is the branching fraction of the $\Upsilon(nS)$ state to the $\mu^+\mu^-$ final state, and \mathcal{L} is the integrated luminosity of the data sample. The values of the branching fractions used in this measurement are $(2.48 \pm 0.05)\%$ for $\Upsilon(1S) \rightarrow \mu^+\mu^-$, $(1.93 \pm 0.17)\%$ for $\Upsilon(2S) \rightarrow \mu^+\mu^-$, and $(2.18 \pm 0.21)\%$ for $\Upsilon(3S) \rightarrow \mu^+\mu^-$ [46].

The nuclear modification factor for ${}^{208}\text{Pb}$ is defined for the $p\text{Pb}$ and Pbp configurations as

$$R_{p\text{Pb}}(p_{\text{T}}, y^*) = \frac{1}{208} \frac{d^2\sigma_{p\text{Pb}}(p_{\text{T}}, y^*)/dp_{\text{T}}dy^*}{d^2\sigma_{pp}(p_{\text{T}}, y^*)/dp_{\text{T}}dy^*}, \quad (2)$$

where σ_{pp} is the reference cross-section from pp collisions interpolated to $\sqrt{s} = 8.16 \text{ TeV}$ using the LHCb measurements at $\sqrt{s} = 2.76, 7, 8$, and 13 TeV .

The forward-to-backward ratio is defined as

$$R_{\text{FB}}(p_{\text{T}}, |y^*|) = \frac{d^2\sigma_{p\text{Pb}}(p_{\text{T}}, +|y^*|)/dp_{\text{T}}dy^*}{d^2\sigma_{p\text{Pb}}(p_{\text{T}}, -|y^*|)/dp_{\text{T}}dy^*}, \quad (3)$$

and is evaluated in the rapidity range of $2.5 < |y^*| < 4.0$, which is common to $p\text{Pb}$ and Pbp collisions.

The ratio of excited $\Upsilon(2S)$ and $\Upsilon(3S)$ states to the $\Upsilon(1S)$ ground state in proton-lead collisions is defined as

$$R(\Upsilon(nS)) = \frac{[d^2\sigma/dp_{\text{T}}dy^*](\Upsilon(nS))}{[d^2\sigma/dp_{\text{T}}dy^*](\Upsilon(1S))}. \quad (4)$$

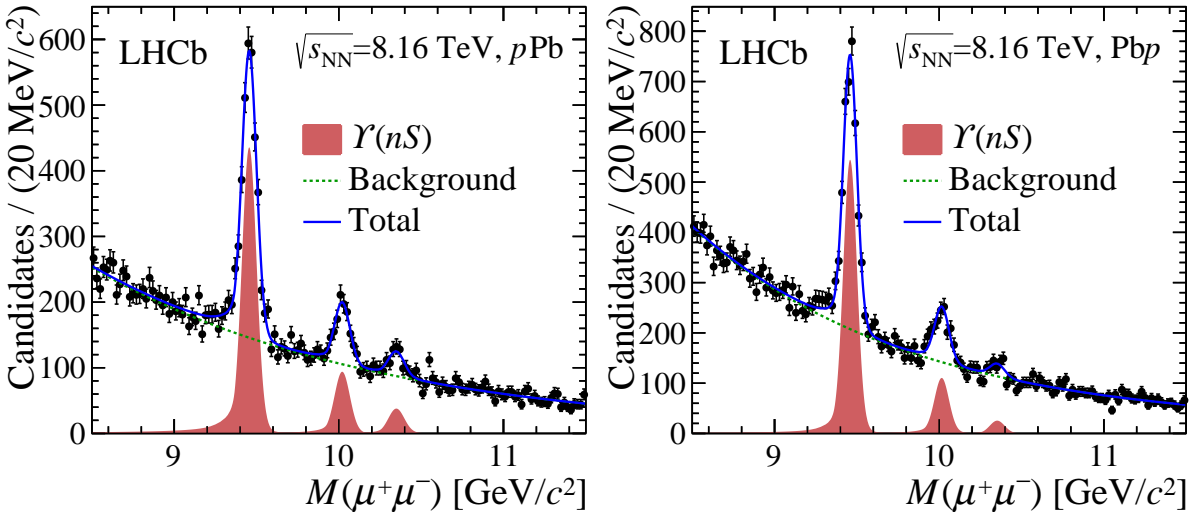


Figure 1: Invariant-mass distribution of $\mu^+\mu^-$ pairs from the (left) $p\text{Pb}$ and (right) Pbp samples after the trigger and offline selections.

In addition, the ratio of $\Upsilon(1S)$ to non-prompt J/ψ cross-sections in proton-lead collisions is measured in the same way. The double ratio

$$\mathfrak{R}_{(p\text{Pb}|\text{Pbp})/pp}^{\Upsilon(nS)/\Upsilon(1S)} = \frac{R(\Upsilon(nS))_{p\text{Pb}|\text{Pbp}}}{R(\Upsilon(nS))_{pp}} \quad (5)$$

compares the ratio $R(\Upsilon(nS))$ in $p\text{Pb}$ or Pbp collisions to $R(\Upsilon(nS))$ in pp collisions.

4 Event selection

The candidates reconstructed in the trigger are further filtered by means of an offline selection. In the offline selection, muon tracks are required to have $p_T > 1 \text{ GeV}/c$, to be in the geometrical acceptance of the spectrometer ($2.0 < \eta < 5.0$), to satisfy PID requirements, and to have a good track-fit quality. The dimuon invariant-mass distribution of offline-selected candidates is shown in Fig. 1 for the $p\text{Pb}$ and Pbp samples.

The dimuon invariant-mass distribution is fitted with an exponential function for the background and three separate peaking functions, each consisting of the sum of two Crystal Ball functions [47] for the $\Upsilon(nS)$ peaks. The shape parameters of the double Crystal Ball functions (n and α) are fixed to the values obtained in the simulation. The yields of $\Upsilon(1S)$, $\Upsilon(2S)$, $\Upsilon(3S)$ mesons in the $p\text{Pb}$ and Pbp samples are summarised in Table 1. The probability that the background can produce a fluctuation greater than or equal to the excess observed in data is calculated as the local p -value. For the exponential-background-only fits in the range of $\pm 100 \text{ MeV}/c^2$ around the expected $\Upsilon(3S)$ mass peak, the local p -values are below 10^{-13} in $p\text{Pb}$ sample and below 10^{-7} in Pbp sample.

Table 1: Yields of $\Upsilon(1S)$, $\Upsilon(2S)$, $\Upsilon(3S)$ mesons in $p\text{Pb}$ and Pbp samples as given by the fit. The uncertainties are statistical only.

Samples	$\Upsilon(1S)$	$\Upsilon(2S)$	$\Upsilon(3S)$	\mathcal{L}
$p\text{Pb}$	2705 ± 87	584 ± 49	262 ± 44	12.5 nb^{-1}
Pbp	3072 ± 82	679 ± 54	159 ± 39	19.3 nb^{-1}

5 Efficiencies

The signal yields are corrected bin-by-bin by the total efficiencies to obtain the cross-section measurements. The total efficiency ε_{tot} includes contributions from the geometrical acceptance, the tracking and trigger efficiencies, and the efficiency of the selection including the requirement on the PID of the muons. All efficiencies are determined from simulation, apart from the tracking and particle-identification efficiencies, where data are used to correct the efficiencies obtained from the simulation. The same procedure is used for each of the three $\Upsilon(nS)$ states.

The muon tracking efficiency is calculated using simulated $\Upsilon(nS)$ events in $p\text{Pb}$ and Pbp collisions, and the efficiency in simulation is calibrated using efficiencies estimated from J/ψ candidates selected in $p\text{Pb}$ data using a tag-and-probe method similar to that adopted in the measurement of J/ψ production using the same data set [29].

The PID efficiency for muons is measured using a statistically independent sample of J/ψ decays in $p\text{Pb}$ and pp data. In regions where the number of J/ψ decays is small, the efficiency is determined using weighted data from pp collisions to reproduce the kinematics and detector occupancies of $p\text{Pb}$ collisions.

The total efficiency for the $\Upsilon(1S)$ state is shown in Fig. 2. The efficiencies for the $\Upsilon(2S)$ and $\Upsilon(3S)$ states are similar. The uncertainties shown are statistical, due to the limited size of the simulated samples, and systematic, which will be discussed in the next section. The difference in efficiencies as a function of rapidity is largely due to acceptance effects.

6 Systematic uncertainties

Table 2 summarises the systematic uncertainties, which are different for each of the $\Upsilon(nS)$ states. The finite size of the simulation samples leads to an uncertainty on the efficiency estimation, which is uncorrelated among bins and $\Upsilon(nS)$ states and contributes to the uncertainties in acceptance, offline selection and trigger efficiencies. These uncertainties are small compared to the other systematic uncertainties and barely affect the overall systematic uncertainty. All other uncertainties are correlated among bins.

The choice of the fit model for the mass distributions affects the signal yields. The uncertainty associated with the choice of the fit functions is estimated using different functions (single Crystal Ball functions for signal, and a second-order polynomial for background), and by modifying the fit range for the signal fit to account for the uncertainty due to the radiative tail. The uncertainty due to the choice of the fit models is estimated to be 5.7%.

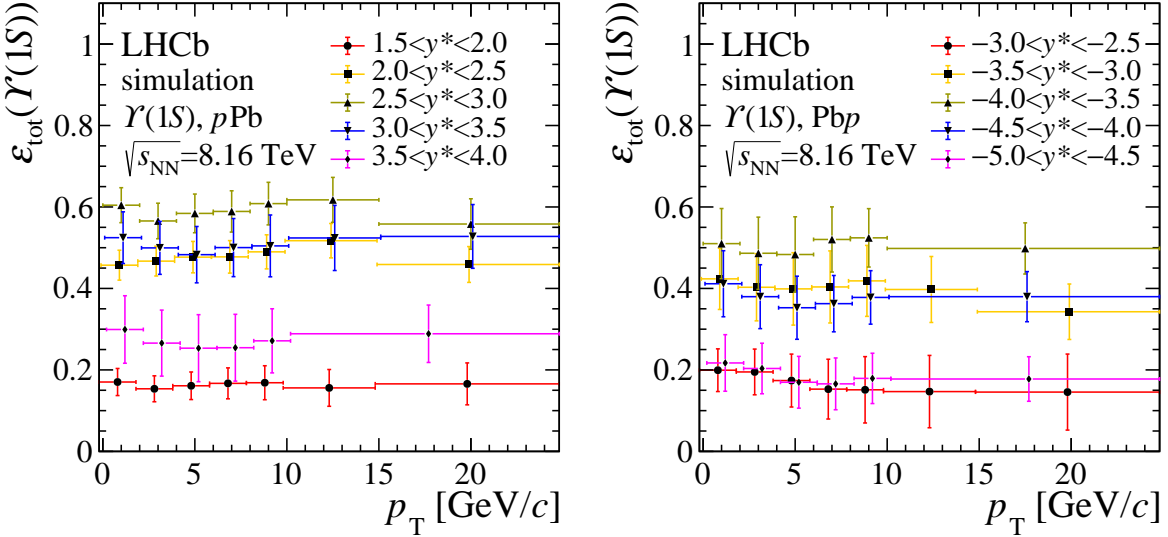


Figure 2: Total efficiency ε_{tot} of the $\Upsilon(1S)$ meson as a function of its p_{T} in different y^* bins in (left) $p\text{Pb}$ and (right) Pbp collisions. The horizontal locations of the markers are roughly the centroids of the bins, with offsets from centre to aid in readability.

Table 2: Systematic uncertainties (in percent) on the cross-section measurements. The ranges indicate the minimum and maximum values in different bins, among all $\Upsilon(nS)$ states.

Source	$p\text{Pb}$	Pbp
Signal determination	5.7%	5.7%
Acceptance	0.7% – 3.4%	0.5% – 3.5%
Reconstruction efficiency	2.1% – 7.9%	2.5% – 8.1%
Offline selection efficiency	0.1% – 0.8%	0.1% – 1.4%
PID efficiency	1.1% – 4.4%	1.9% – 6.0%
Trigger efficiency	2.0% – 2.8%	2.0% – 2.4%
Luminosity	2.6%	2.5%
Branching ratio	2.0% – 9.6%	2.0% – 9.6%

The track reconstruction efficiency calibration has uncertainties from three sources: the size of the calibration samples, the selection efficiency, and the signal yield determination of the calibration data sample. Considering all these effects, the total uncertainty from the reconstruction of the tracks varies from 2.1% to 7.9% for the $p\text{Pb}$ sample and from 2.5% to 8.1% for the Pbp sample.

The uncertainty on the offline selection efficiency is only due to the finite size of the simulation sample, varying from 0.1% to 1.4%.

The PID uncertainties are related to the limited size of the pp and $p\text{Pb}$ (Pbp) calibration samples, and to the difference between the pp and $p\text{Pb}$ (Pbp) PID calibration samples. The latter effects lead to an uncertainty on the PID efficiency varying from 1.1% to 3.9% for the $p\text{Pb}$ sample and from 1.9% to 2.8% for the Pbp sample. The total PID uncertainty

including all effects varies from 1.1% to 4.4% for the $p\text{Pb}$ sample and from 1.9% to 6.0% for the $\text{P}p\text{p}$ sample.

The trigger efficiency is obtained from simulation. The limited size of the simulated samples contributes to kinematic-bin-dependent uncertainties that vary between 0.2% and 2.0% for the $p\text{Pb}$ sample and between 0.2% and 1.2% in the $\text{P}p\text{p}$ sample. An additional uncertainty of 2.0% is assigned based on a study of the trigger efficiency on a calibration data sample.

The relative uncertainty on the $p\text{Pb}$ luminosity determined by the van der Meer scan is 2.6% and that on the $\text{P}p\text{p}$ luminosity is 2.5%.

The uncertainties from the decay branching fractions of the $\Upsilon(nS)$ states contribute to the systematic uncertainty for values between 2.0 and 9.6% [46].

7 Results

The total $\Upsilon(nS)$ cross-sections in the kinematic region $p_{\text{T}} < 25 \text{ GeV}/c$ and $1.5 < y^* < 4.0$ ($-5.0 < y^* < -2.5$) for $p\text{Pb}$ ($\text{P}p\text{p}$) sample are measured to be

$$\begin{aligned}\sigma_{p\text{Pb}}^{\Upsilon(1S)} &= 22.8 \pm 0.9 \text{ (stat)} \pm 2.1 \text{ (syst)} \mu\text{b}, \\ \sigma_{p\text{Pb}}^{\Upsilon(2S)} &= 6.4 \pm 0.6 \text{ (stat)} \pm 0.8 \text{ (syst)} \mu\text{b}, \\ \sigma_{p\text{Pb}}^{\Upsilon(3S)} &= 2.5 \pm 0.4 \text{ (stat)} \pm 0.3 \text{ (syst)} \mu\text{b}, \\ \sigma_{\text{P}p\text{p}}^{\Upsilon(1S)} &= 20.3 \pm 0.8 \text{ (stat)} \pm 2.6 \text{ (syst)} \mu\text{b}, \\ \sigma_{\text{P}p\text{p}}^{\Upsilon(2S)} &= 6.0 \pm 0.5 \text{ (stat)} \pm 0.9 \text{ (syst)} \mu\text{b}, \\ \sigma_{\text{P}p\text{p}}^{\Upsilon(3S)} &= 1.2 \pm 0.3 \text{ (stat)} \pm 0.2 \text{ (syst)} \mu\text{b}.\end{aligned}$$

The cross-sections are also evaluated as a function of p_{T} and y^* for the $\Upsilon(1S)$ and $\Upsilon(2S)$ states. The double-differential cross-section for the $\Upsilon(1S)$ state is shown in Fig. 3. It is integrated over p_{T} to form a differential cross-section as a function of y^* , as shown in Fig. 4 (left), and integrated over y^* to form a differential cross-section as a function of p_{T} , as shown in Fig. 5 (left).¹ Similarly, for the $\Upsilon(2S)$ state the differential cross-section as a function of y^* and p_{T} are shown in Fig. 4 (right) and Fig. 5 (right), respectively. For the $\Upsilon(3S)$ state, due to the limited sample size, only the cross-section integrated over p_{T} and y^* is measured.

To measure the nuclear modification factor, a measurement of the pp cross-section at the same centre-of-mass energy is needed. In the absence of a direct measurement, the value of the $\Upsilon(nS)$ cross-section in pp collisions at $\sqrt{s} = 8.16 \text{ TeV}$ is obtained by interpolating between the values measured in pp collisions by LHCb at 2.76, 7, 8 and 13 TeV [48–50] using a second-order polynomial function. The differences between the scale factors obtained using the nominal second-order polynomial fits and alternative fits using exponential functions are assigned as systematic uncertainties on the interpolated cross-sections. The values of the $\Upsilon(1S)$ and $\Upsilon(2S)$ differential cross-sections in p_{T} (y^*) integrated over y^* (p_{T}) in pp collisions at $\sqrt{s} = 8.16 \text{ TeV}$ are shown in Figs. 4 to 5, and their numerical values are provided in Appendix B. The production of both $\Upsilon(1S)$ and

¹ The numerical results of all cross-section measurements shown in this section can be found in Appendix A.

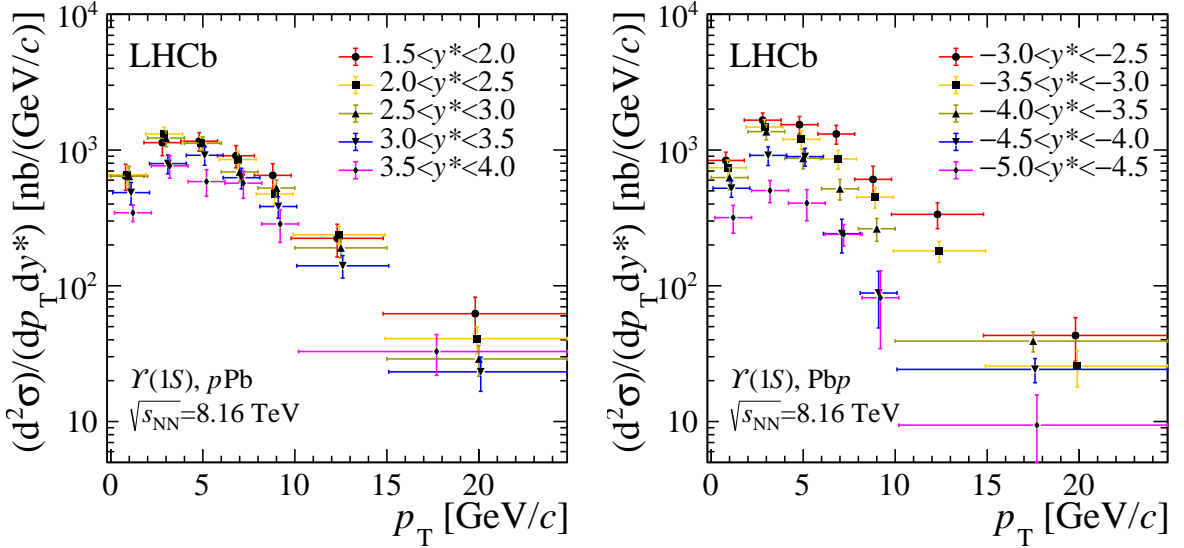


Figure 3: Double-differential cross-section for the $\Upsilon(1S)$ meson as a function of p_T for different values of y^* for the (left) forward $p\text{Pb}$ and (right) backward $\text{Pb}p$ samples. The uncertainties are the sums in quadrature of the statistical and systematic components. The horizontal locations of the markers are roughly the centroids of the bins, with offsets from centre to aid in readability.

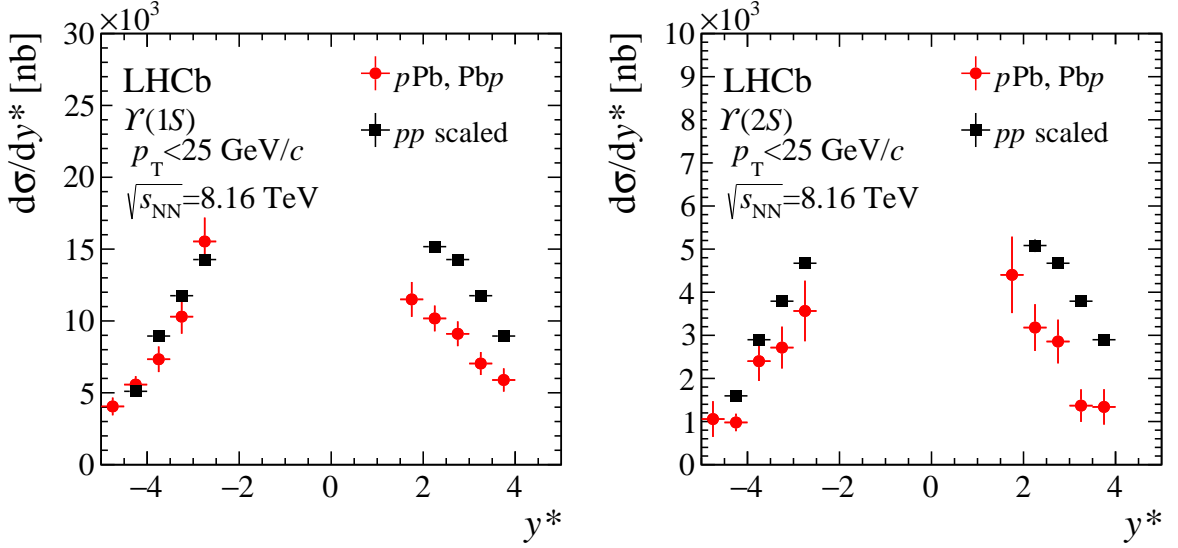


Figure 4: Cross-section of (left) $\Upsilon(1S)$ and (right) $\Upsilon(2S)$ production as a function of y^* integrated over p_T for the backward (negative y^*) and forward (positive y^*) samples, compared to the cross-section measured in pp , interpolated to $\sqrt{s_{\text{NN}}} = 8.16 \text{ TeV}$. In this and subsequent figures, the uncertainties shown are the sums in quadrature of the statistical and systematic components.

$\Upsilon(2S)$ is suppressed in the forward $p\text{Pb}$ region with respect to the scaled value from pp collisions, as already observed in the prompt J/ψ measurement [29], while no significant suppression is visible in the backward $\text{Pb}p$ region. The nuclear modification factors are

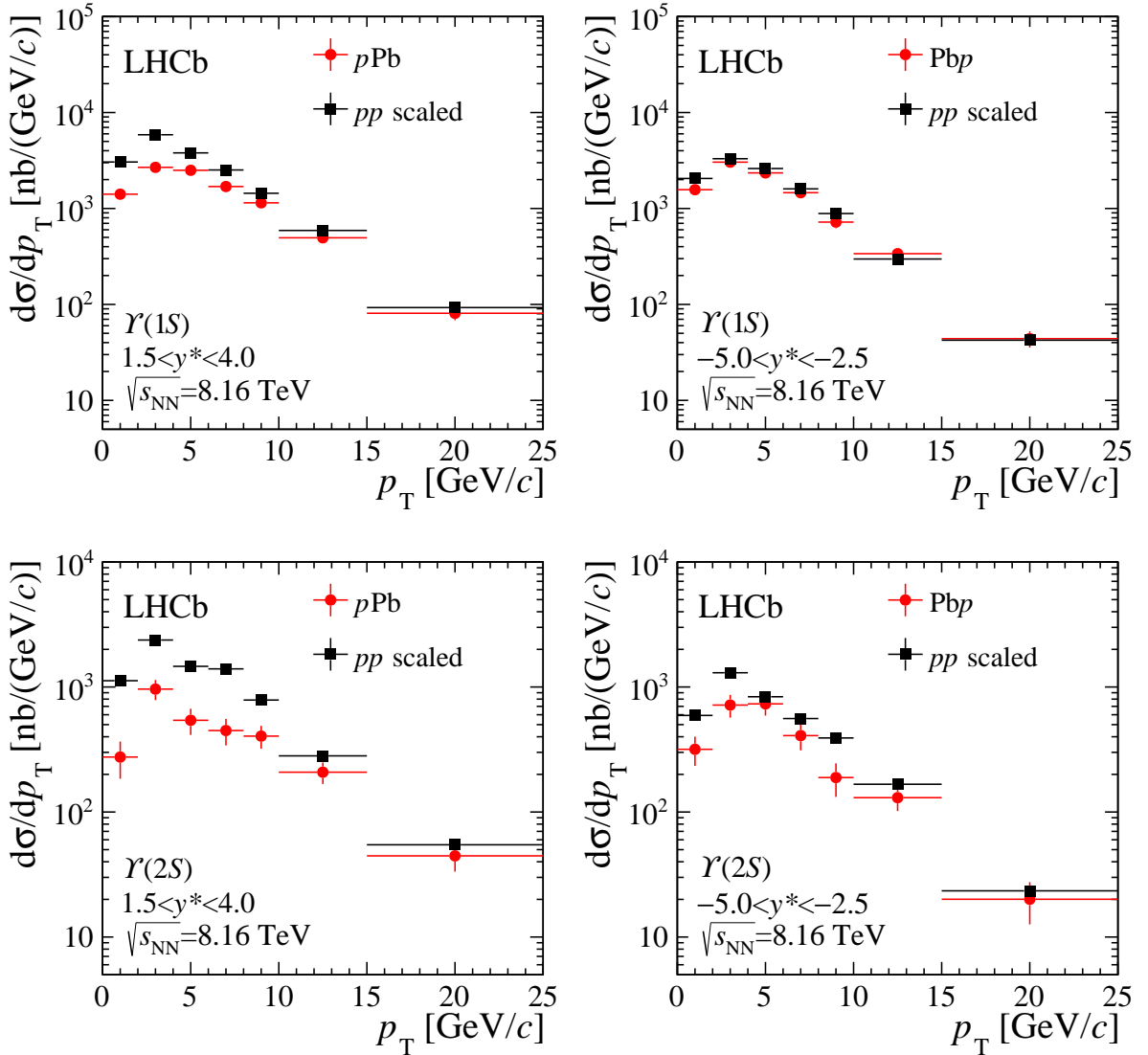


Figure 5: Cross-section of (top) $\Upsilon(1S)$ and (bottom) $\Upsilon(2S)$ production as a function of p_T integrated over y^* for the (left) forward and (right) backward samples compared to the cross-section measured in pp , interpolated to $\sqrt{s_{NN}} = 8.16$ TeV.

evaluated as functions of p_T and y^* for the $\Upsilon(1S)$ and $\Upsilon(2S)$ states,² and compared with different theoretical calculations:

1. A calculation based on the “HELAC-Onia” framework [51–53], where the modification of the parton flux due to CNM is treated within the collinear factorisation framework using two different nuclear parton distribution functions (nPDFs), the EPPS16 NNPDF [54] and nCTEQ15 set [7].
2. Calculations based on the *comovers* model of $\Upsilon(nS)$ production [17, 18], which implements final state interaction of the quarkonia states and nuclear parton distribution

² In the nuclear modification factors, the systematic uncertainty related to branching ratios cancels.

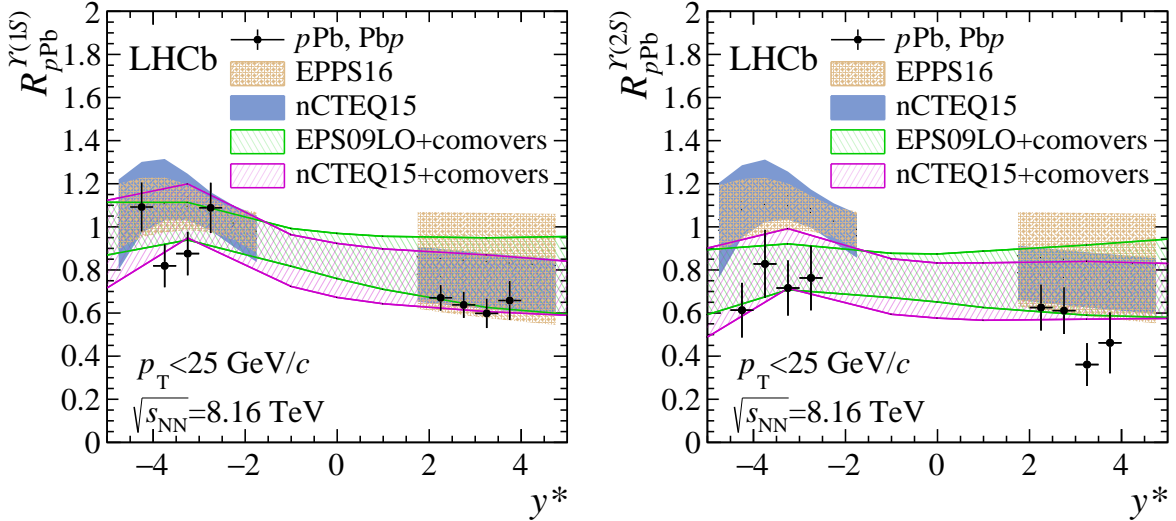


Figure 6: Nuclear modification factors of the (left) $\Upsilon(1S)$ and (right) $\Upsilon(2S)$ mesons as a function of y^* integrated over p_T for the forward and backward samples. The bands correspond to the theoretical predictions for the nCTEQ15 and EPPS16 NNPDF sets, and the comovers model as reported in the text.

function modification via EPS09 at leading order [6], and the nCTEQ15 set already described.

The measurements and the calculations are shown in Figs. 6 and 7. For the $\Upsilon(1S)$ state the nuclear modification factor is about 0.5 (0.8) at low p_T in the forward (backward) region, and is consistent with unity for p_T larger than 10 GeV/c, as predicted by the models. As a function of rapidity, R_{pPb} is consistent with unity in the Pbp region at negative $|y^*|$, while a suppression is observed in the pPb region, where it averages around 0.7, consistent with the models analysed. The nuclear modification factor for $\Upsilon(2S)$ is smaller than $\Upsilon(1S)$, which is consistent with the comovers models. The corresponding numerical results can be found in Appendix C. The same trend as for the $\Upsilon(1S)$ state is observed for the $\Upsilon(2S)$ state, although the suppression seems more pronounced for the $\Upsilon(2S)$ state, as already observed by other experiments [22], especially in the backward region.

The forward-backward asymmetry is evaluated only for the $\Upsilon(1S)$ meson as a function of p_T and y^* , see Fig. 8, whereas for the $\Upsilon(2S)$ meson it is integrated over both y^* and p_T as shown in Fig. 9. The corresponding numerical results can be found in Appendix D.³

The ratio of the cross-sections of $\Upsilon(2S)$ and $\Upsilon(1S)$ mesons as a function of p_T , integrated over y^* , and as function of y^* , integrated over p_T , are shown in Fig. 10. The corresponding numerical results can be found in Appendix E. The ratios confirmed a larger suppression for the excited states with respect to the ground state observed in proton-lead collisions compared to pp collisions [49]. For the $\Upsilon(3S)$ state, due to the limited size of the data sample, only an integral ratio is measured. In the determination of the ratio $R(\Upsilon(nS))$, most of the systematic uncertainties cancel, except that related to

³In the forward-backward ratio, the systematic uncertainty related to branching ratios cancels.

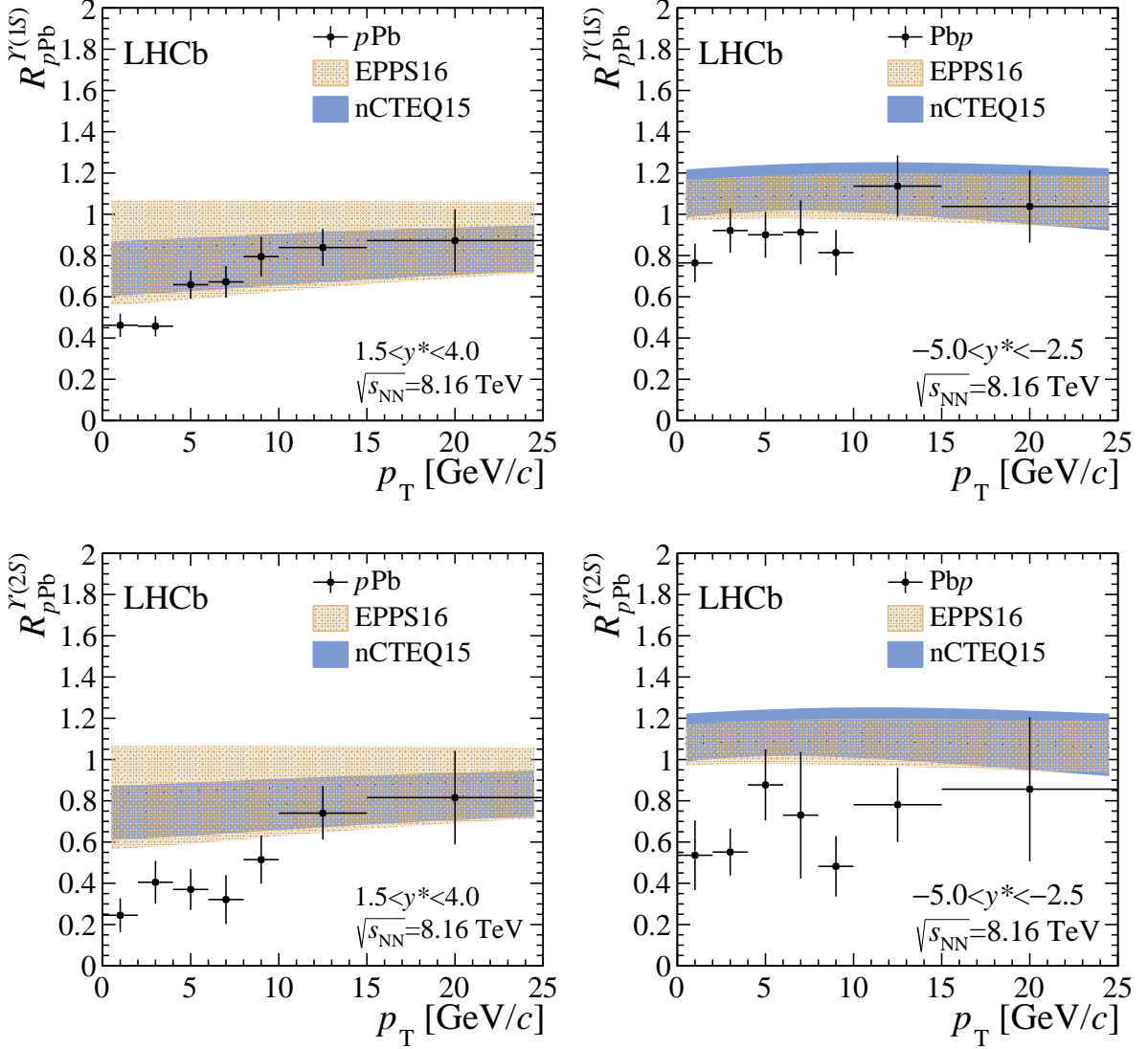


Figure 7: Nuclear modification factors of the (top) $\Upsilon(1S)$ and (bottom) $\Upsilon(2S)$ mesons as a function of p_T integrated over y^* for the (left) forward and (right) backward samples. The bands correspond to the theoretical predictions for the nCTEQ15 and EPPS16 NNPDF sets as reported in the text.

branching ratios.

The integrated ratios are summarised in Table 3, where values are also reported for pp collisions. The corresponding double-ratio results are shown in Fig. 11 (left), together with the comovers model calculations, and the numerical results are

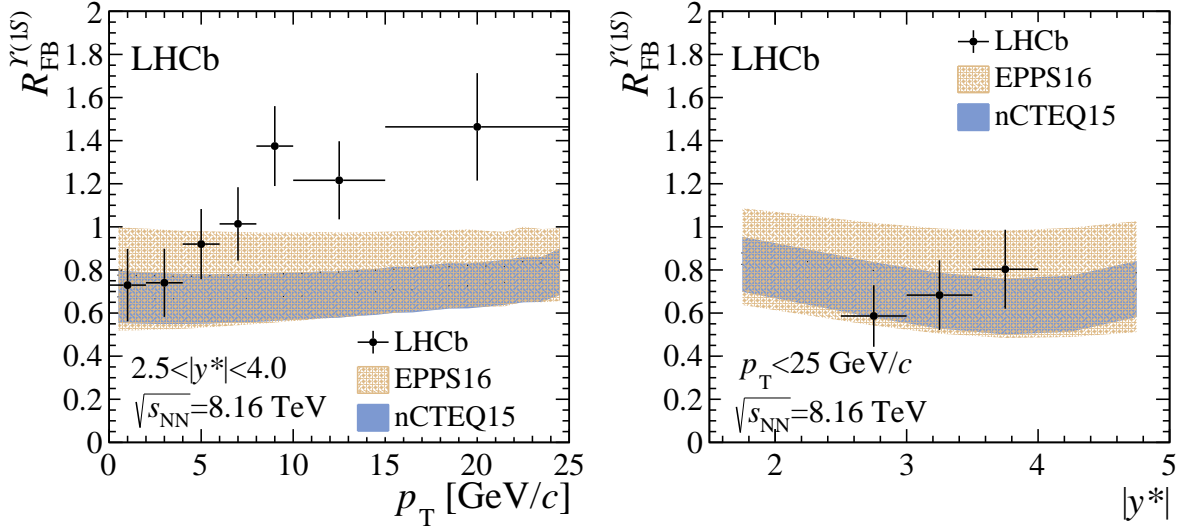


Figure 8: Forward-backward ratio for the $\Upsilon(1S)$ as a function of (left) p_T integrated over y^* and (right) as a function of $|y^*|$ integrated over p_T . The bands correspond to the theoretical calculations for the nCTEQ15 and EPPS16 NNPDF sets as reported in the text.

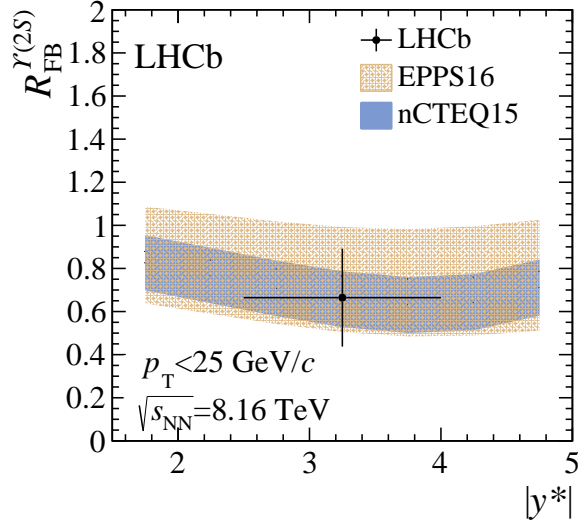


Figure 9: Forward-backward ratio for the $\Upsilon(2S)$ compared with theoretical calculations for the nCTEQ15 and EPPS16 NNPDF sets as reported in the text.

$$\begin{aligned}
 \Re_{p\text{Pb}/pp}^{\Upsilon(2S)/\Upsilon(1S)} &= 0.86 \pm 0.15, \\
 \Re_{p\text{Pb}/pp}^{\Upsilon(3S)/\Upsilon(1S)} &= 0.81 \pm 0.15, \\
 \Re_{\text{Pb}p/pp}^{\Upsilon(2S)/\Upsilon(1S)} &= 0.91 \pm 0.21, \\
 \Re_{\text{Pb}p/pp}^{\Upsilon(3S)/\Upsilon(1S)} &= 0.44 \pm 0.15.
 \end{aligned}$$

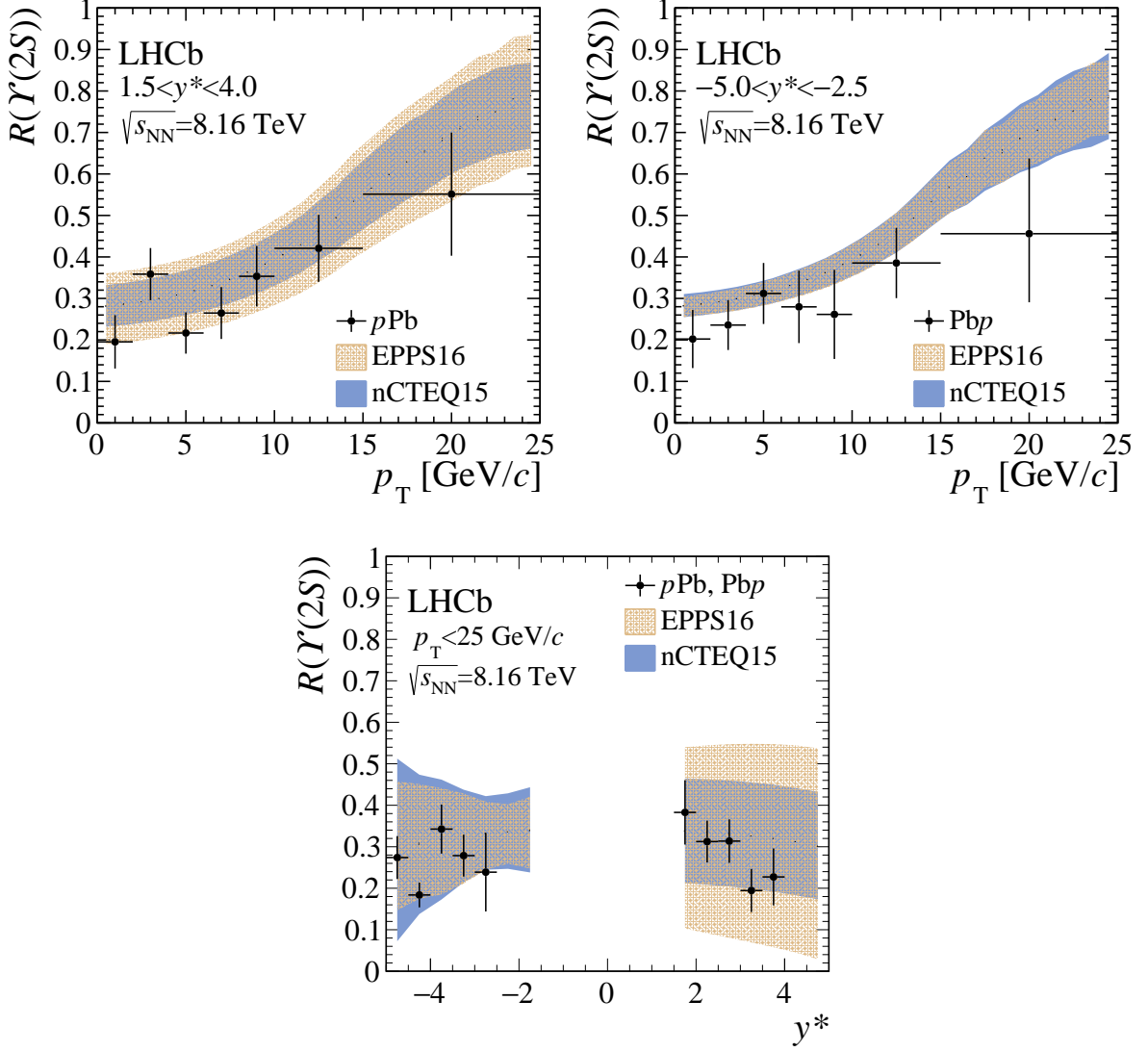


Figure 10: Ratios between $\Upsilon(2S)$ and $\Upsilon(1S)$ cross-sections as a function of (top) p_T integrated over y^* , and as function of (bottom) y^* integrated over p_T , for $p\text{Pb}$ and Pbp collisions. The bands correspond to the theoretical predictions for the nCTEQ15 and EPPS16 NNPDF sets as reported in the text.

For the double ratio of the $\Upsilon(3S)$ over $\Upsilon(1S)$ in the backward a clear indication of stronger suppression is observed, in agreement with the comovers model as shown in Fig. 11 (right). The ratio of the $\Upsilon(1S)$ and nonprompt J/ψ cross-sections in $p\text{Pb}$ and Pbp collisions is also measured, where the the nonprompt J/ψ cross-section was measured previously by LHCb [29] using the same data sample. The ratio is shown in Fig. 12 compared to the corresponding result observed in pp collisions. The numerical results are reported in Appendix F. A small suppression is visible, which could be attributed to final-state CNM effects. More data are needed in order to have a more definite indication of a different suppression mechanism for bottomonium and open beauty, such as $\Upsilon(1S)$ and nonprompt J/ψ states, as indicated by Refs. [55, 56].

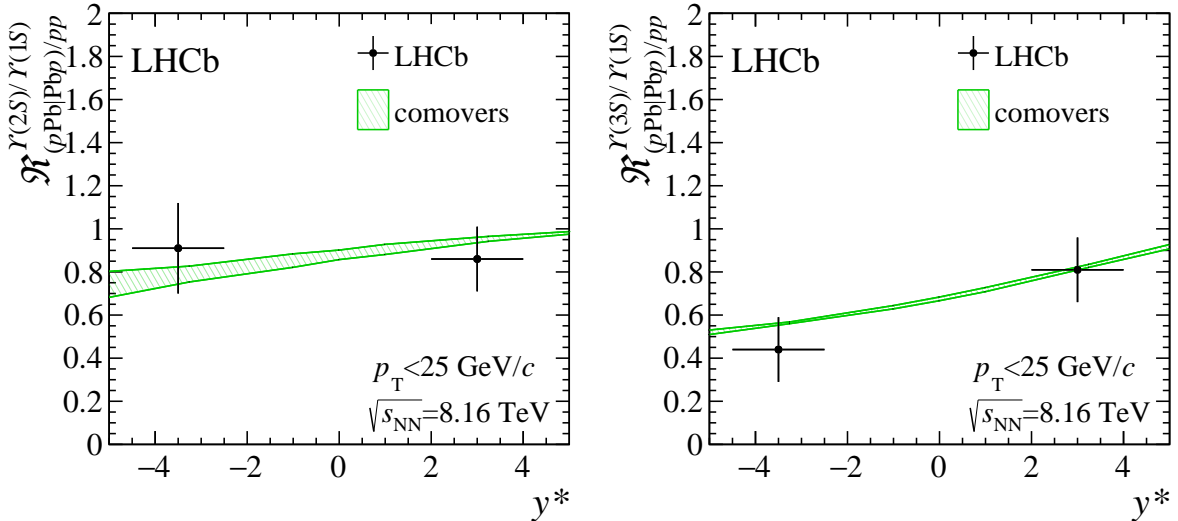


Figure 11: Double ratios for (left) $\Upsilon(2S)$ and (right) $\Upsilon(3S)$. The bands correspond to the theoretical prediction for the comovers model as reported in the text.

Table 3: Ratio $R(\Upsilon(nS))$ in pp , $p\text{Pb}$, and $\text{Pb}p$ samples. The uncertainties are combinations of statistical and systematical components.

Sample	$R(\Upsilon(2S))$	$R(\Upsilon(3S))$
pp $2.0 < y^* < 4.0$	0.328 ± 0.004	0.137 ± 0.002
pp $-4.5 < y^* < -2.5$	0.325 ± 0.004	0.137 ± 0.002
$p\text{Pb}$ $2.0 < y^* < 4.0$	0.282 ± 0.049	0.111 ± 0.021
$\text{Pb}p$ $-4.5 < y^* < -2.5$	0.296 ± 0.070	0.060 ± 0.016

8 Summary

The production of $\Upsilon(nS)$ states is studied in proton-lead collisions at $\sqrt{s_{\text{NN}}} = 8.16$ TeV using data collected by the LHCb detector in 2016. The cross-sections, nuclear modification factors and forward-backward ratios are measured double-differentially ($\Upsilon(1S)$) and single-differentially ($\Upsilon(2S)$). The ratios of the production cross-sections of the different $\Upsilon(nS)$ states are also measured as functions of transverse momentum and rapidity in the nucleon-nucleon centre-of-mass frame. The results are consistent with previous observations and with the theoretical model calculations, indicating some suppression of $\Upsilon(nS)$ production in proton-lead collisions, more pronounced for the excited Υ states.

Acknowledgements

We thank the theorists who provided predictions for our measurements: J.-P. Lansberg, H.-S. Shao and E. Gonzalez-Ferreiro. We express our gratitude to our colleagues in the CERN accelerator departments for the excellent performance of the LHC. We thank the technical

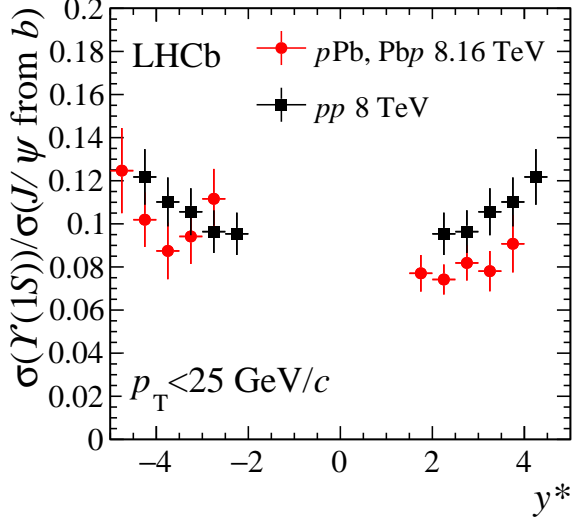


Figure 12: Ratio of $\Upsilon(1S)$ to nonprompt J/ψ cross-sections as a function of y^* integrated over p_T , for $p\text{Pb}$ and $\text{Pb}p$ collisions.

and administrative staff at the LHCb institutes. We acknowledge support from CERN and from the national agencies: CAPES, CNPq, FAPERJ and FINEP (Brazil); MOST and NSFC (China); CNRS/IN2P3 (France); BMBF, DFG and MPG (Germany); INFN (Italy); NWO (Netherlands); MNiSW and NCN (Poland); MEN/IFA (Romania); MSHE (Russia); MinECo (Spain); SNSF and SER (Switzerland); NASU (Ukraine); STFC (United Kingdom); NSF (USA). We acknowledge the computing resources that are provided by CERN, IN2P3 (France), KIT and DESY (Germany), INFN (Italy), SURF (Netherlands), PIC (Spain), GridPP (United Kingdom), RRCKI and Yandex LLC (Russia), CSCS (Switzerland), IFIN-HH (Romania), CBPF (Brazil), PL-GRID (Poland) and OSC (USA). We are indebted to the communities behind the multiple open-source software packages on which we depend. Individual groups or members have received support from AvH Foundation (Germany); EPLANET, Marie Skłodowska-Curie Actions and ERC (European Union); ANR, Labex P2IO and OCEVU, and Région Auvergne-Rhône-Alpes (France); Key Research Program of Frontier Sciences of CAS, CAS PIFI, and the Thousand Talents Program (China); RFBR, RSF and Yandex LLC (Russia); GVA, XuntaGal and GENCAT (Spain); the Royal Society and the Leverhulme Trust (United Kingdom); Laboratory Directed Research and Development program of LANL (USA).

Appendices

A Cross-section

Tables 4 and 5 list the double-differential cross-section for $\Upsilon(1S)$ in $p\text{Pb}$ forward and backward samples. Tables 6 and 7 list the differential cross-section for $\Upsilon(1S)$ in bins of transverse momentum and rapidity. The corresponding values for the $\Upsilon(2S)$ state are listed in Tables 8 and 9. In all tables, the quoted uncertainties are the sum in quadrature of the statistical and systematic components.

Table 4: $\Upsilon(1S)$ production cross-section in $p\text{Pb}$, as a function of p_{T} and y^* .

p_{T} [GeV/ c]	y^*	$\frac{d^2\sigma}{dp_{\text{T}}dy^*}$ [nb/(GeV/ c)]
$0 < p_{\text{T}} < 2$	$1.5 < y^* < 2.0$	644 ± 142
$0 < p_{\text{T}} < 2$	$2.0 < y^* < 2.5$	656 ± 106
$0 < p_{\text{T}} < 2$	$2.5 < y^* < 3.0$	641 ± 119
$0 < p_{\text{T}} < 2$	$3.0 < y^* < 3.5$	486 ± 92
$0 < p_{\text{T}} < 2$	$3.5 < y^* < 4.0$	345 ± 50
$2 < p_{\text{T}} < 4$	$1.5 < y^* < 2.0$	1134 ± 227
$2 < p_{\text{T}} < 4$	$2.0 < y^* < 2.5$	1312 ± 163
$2 < p_{\text{T}} < 4$	$2.5 < y^* < 3.0$	1226 ± 171
$2 < p_{\text{T}} < 4$	$3.0 < y^* < 3.5$	794 ± 129
$2 < p_{\text{T}} < 4$	$3.5 < y^* < 4.0$	765 ± 147
$4 < p_{\text{T}} < 6$	$1.5 < y^* < 2.0$	1162 ± 184
$4 < p_{\text{T}} < 6$	$2.0 < y^* < 2.5$	1130 ± 128
$4 < p_{\text{T}} < 6$	$2.5 < y^* < 3.0$	1121 ± 135
$4 < p_{\text{T}} < 6$	$3.0 < y^* < 3.5$	915 ± 147
$4 < p_{\text{T}} < 6$	$3.5 < y^* < 4.0$	586 ± 132
$6 < p_{\text{T}} < 8$	$1.5 < y^* < 2.0$	908 ± 171
$6 < p_{\text{T}} < 8$	$2.0 < y^* < 2.5$	851 ± 135
$6 < p_{\text{T}} < 8$	$2.5 < y^* < 3.0$	690 ± 106
$6 < p_{\text{T}} < 8$	$3.0 < y^* < 3.5$	625 ± 111
$6 < p_{\text{T}} < 8$	$3.5 < y^* < 4.0$	570 ± 131
$8 < p_{\text{T}} < 10$	$1.5 < y^* < 2.0$	651 ± 145
$8 < p_{\text{T}} < 10$	$2.0 < y^* < 2.5$	474 ± 83
$8 < p_{\text{T}} < 10$	$2.5 < y^* < 3.0$	525 ± 79
$8 < p_{\text{T}} < 10$	$3.0 < y^* < 3.5$	384 ± 71
$8 < p_{\text{T}} < 10$	$3.5 < y^* < 4.0$	285 ± 79
$10 < p_{\text{T}} < 15$	$1.5 < y^* < 2.0$	224 ± 61
$10 < p_{\text{T}} < 15$	$2.0 < y^* < 2.5$	237 ± 36
$10 < p_{\text{T}} < 15$	$2.5 < y^* < 3.0$	190 ± 30
$10 < p_{\text{T}} < 15$	$3.0 < y^* < 3.5$	140 ± 28
$10 < p_{\text{T}} < 25$	$3.5 < y^* < 4.0$	33 ± 11
$15 < p_{\text{T}} < 25$	$1.5 < y^* < 2.0$	62 ± 20
$15 < p_{\text{T}} < 25$	$2.0 < y^* < 2.5$	41 ± 9
$15 < p_{\text{T}} < 25$	$2.5 < y^* < 3.0$	29 ± 8
$15 < p_{\text{T}} < 25$	$3.0 < y^* < 3.5$	23 ± 7

Table 5: $\Upsilon(1S)$ production cross-section in Pbp , as a function of p_T and y^* .

p_T [GeV/c]	y^*	$\frac{d^2\sigma}{dp_T dy^*}$ [nb/(GeV/c)]
$0 < p_T < 2$	$-3.0 < y^* < -2.5$	839 ± 130
$0 < p_T < 2$	$-3.5 < y^* < -3.0$	740 ± 114
$0 < p_T < 2$	$-4.0 < y^* < -3.5$	627 ± 129
$0 < p_T < 2$	$-4.5 < y^* < -4.0$	523 ± 90
$0 < p_T < 2$	$-5.0 < y^* < -4.5$	318 ± 77
$2 < p_T < 4$	$-3.0 < y^* < -2.5$	1661 ± 228
$2 < p_T < 4$	$-3.5 < y^* < -3.0$	1478 ± 225
$2 < p_T < 4$	$-4.0 < y^* < -3.5$	1366 ± 216
$2 < p_T < 4$	$-4.5 < y^* < -4.0$	913 ± 164
$2 < p_T < 4$	$-5.0 < y^* < -4.5$	503 ± 99
$4 < p_T < 6$	$-3.0 < y^* < -2.5$	1538 ± 243
$4 < p_T < 6$	$-3.5 < y^* < -3.0$	1199 ± 204
$4 < p_T < 6$	$-4.0 < y^* < -3.5$	869 ± 165
$4 < p_T < 6$	$-4.5 < y^* < -4.0$	895 ± 152
$4 < p_T < 6$	$-5.0 < y^* < -4.5$	406 ± 107
$6 < p_T < 8$	$-3.0 < y^* < -2.5$	1313 ± 222
$6 < p_T < 8$	$-3.5 < y^* < -3.0$	859 ± 149
$6 < p_T < 8$	$-4.0 < y^* < -3.5$	518 ± 99
$6 < p_T < 8$	$-4.5 < y^* < -4.0$	242 ± 69
$6 < p_T < 8$	$-5.0 < y^* < -4.5$	240 ± 45
$8 < p_T < 10$	$-3.0 < y^* < -2.5$	608 ± 156
$8 < p_T < 10$	$-3.5 < y^* < -3.0$	449 ± 83
$8 < p_T < 10$	$-4.0 < y^* < -3.5$	263 ± 53
$8 < p_T < 10$	$-4.5 < y^* < -4.0$	88 ± 40
$8 < p_T < 10$	$-5.0 < y^* < -4.5$	82 ± 47
$10 < p_T < 15$	$-3.0 < y^* < -2.5$	336 ± 75
$10 < p_T < 15$	$-3.5 < y^* < -3.0$	181 ± 33
$10 < p_T < 25$	$-4.0 < y^* < -3.5$	39 ± 7
$10 < p_T < 25$	$-4.5 < y^* < -4.0$	24 ± 5
$10 < p_T < 25$	$-5.0 < y^* < -4.5$	9 ± 6
$15 < p_T < 25$	$-3.0 < y^* < -2.5$	43 ± 15
$15 < p_T < 25$	$-3.5 < y^* < -3.0$	26 ± 8

Table 6: $\Upsilon(1S)$ production cross-section in $p\text{Pb}$ and Pbp , as a function of p_{T} .

p_{T} (GeV/ c)	$\frac{d\sigma}{dp_{\text{T}}}$ in $p\text{Pb}$ [nb/(GeV/ c)]	$\frac{d\sigma}{dp_{\text{T}}}$ in Pbp [nb/(GeV/ c)]
$0 < p_{\text{T}} < 2$	1409 ± 164	1570 ± 234
$2 < p_{\text{T}} < 4$	2683 ± 287	3040 ± 437
$4 < p_{\text{T}} < 6$	2500 ± 268	2349 ± 341
$6 < p_{\text{T}} < 8$	1693 ± 197	1461 ± 203
$8 < p_{\text{T}} < 10$	1145 ± 142	721 ± 107
$10 < p_{\text{T}} < 15$	495 ± 61	338 ± 48
$15 < p_{\text{T}} < 25$	81 ± 13	44 ± 9

Table 7: $\Upsilon(1S)$ production cross-section in $p\text{Pb}$ and Pbp , as a function of y^* .

y^*	$\frac{d\sigma}{dy^*}$ [nb]
$-5.0 < y^* < -4.5$	4050 ± 646
$-4.5 < y^* < -4.0$	5572 ± 720
$-4.0 < y^* < -3.5$	7333 ± 1109
$-3.5 < y^* < -3.0$	10300 ± 1399
$-3.0 < y^* < -2.5$	15531 ± 1868
$1.5 < y^* < 2.0$	11500 ± 1266
$2.0 < y^* < 2.5$	10175 ± 955
$2.5 < y^* < 3.0$	9107 ± 908
$3.0 < y^* < 3.5$	7038 ± 843
$3.5 < y^* < 4.0$	5891 ± 862

Table 8: $\Upsilon(2S)$ production cross-section in $p\text{Pb}$ and Pbp , as a function of p_{T} .

p_{T} [GeV/ c]	$\frac{d\sigma}{dp_{\text{T}}}$ in $p\text{Pb}$ [nb/(GeV/ c)]	$\frac{d\sigma}{dp_{\text{T}}}$ in Pbp [nb/(GeV/ c)]
$0 < p_{\text{T}} < 2$	275 ± 91	317 ± 83
$2 < p_{\text{T}} < 4$	962 ± 179	717 ± 148
$4 < p_{\text{T}} < 6$	542 ± 129	733 ± 142
$6 < p_{\text{T}} < 8$	448 ± 109	409 ± 97
$8 < p_{\text{T}} < 10$	405 ± 86	189 ± 57
$10 < p_{\text{T}} < 15$	208 ± 42	130 ± 28
$15 < p_{\text{T}} < 25$	45 ± 11	20 ± 7

Table 9: $\Upsilon(2S)$ production cross-section in $p\text{Pb}$, as a function of y^* .

y^*	$\frac{d\sigma}{dy^*}$ [nb]
$-5.0 < y^* < -4.5$	1058 ± 414
$-4.5 < y^* < -4.0$	979 ± 202
$-4.0 < y^* < -3.5$	2400 ± 458
$-3.5 < y^* < -3.0$	2716 ± 485
$-3.0 < y^* < -2.5$	3565 ± 702
$1.5 < y^* < 2.0$	4402 ± 898
$2.0 < y^* < 2.5$	3180 ± 551
$2.5 < y^* < 3.0$	2856 ± 515
$3.0 < y^* < 3.5$	1369 ± 381
$3.5 < y^* < 4.0$	1339 ± 416

B Scaled $\Upsilon(1S)$ and $\Upsilon(2S)$ differential cross-sections in pp collisions

Tables 10 and 11 show the $\Upsilon(1S)$ and $\Upsilon(2S)$ differential cross-sections scaled to the cross-section in pp collisions at $\sqrt{s_{\text{NN}}} = 8.16$ TeV in p_T integrated over y in region $2.0 < y < 4.5$ and in y over p_T in region $p_T < 25$ GeV/ c .

Table 10: Scaled pp differential cross-section in p_T at $\sqrt{s_{\text{NN}}} = 8.16$ TeV. The first uncertainty is statistical, the second is systematic, which includes the systematic uncertainty from the pp measurement and that estimated by changing the interpolation function.

p_T [GeV/ c]	$\Upsilon(1S)$ $\frac{d\sigma}{dp_T}$ [nb/(GeV/ c)]	$\Upsilon(2S)$ $\frac{d\sigma}{dp_T}$ [nb/(GeV/ c)]
$0 < p_T < 2$	$1995 \pm 14 \pm 31$	$555 \pm 9 \pm 11$
$2 < p_T < 4$	$3626 \pm 18 \pm 51$	$1052 \pm 11 \pm 19$
$4 < p_T < 6$	$2898 \pm 16 \pm 40$	$910 \pm 11 \pm 15$
$6 < p_T < 8$	$1786 \pm 12 \pm 28$	$634 \pm 9 \pm 14$
$8 < p_T < 10$	$1009 \pm 9 \pm 15$	$394 \pm 7 \pm 7$
$10 < p_T < 15$	$382 \pm 5 \pm 7$	$169 \pm 4 \pm 4$
$15 < p_T < 25$	$54 \pm 2 \pm 1$	$29 \pm 1 \pm 1$

Table 11: Scaled pp differential cross-section in y at $\sqrt{s_{\text{NN}}} = 8.16$ TeV. The first uncertainty is statistical, the second is systematic, which includes the systematic uncertainty from the pp measurement and that estimated by changing the interpolation function.

y	$\Upsilon(1S)$ $\frac{d\sigma}{dy}$ [nb]	$\Upsilon(2S)$ $\frac{d\sigma}{dy}$ [nb]
$2.0 < y < 2.5$	$15171 \pm 143 \pm 250$	$5083 \pm 105 \pm 110$
$2.5 < y < 3.0$	$14273 \pm 82 \pm 193$	$4672 \pm 60 \pm 79$
$3.0 < y < 3.5$	$11758 \pm 66 \pm 170$	$3792 \pm 49 \pm 71$
$3.5 < y < 4.0$	$8950 \pm 65 \pm 137$	$2898 \pm 46 \pm 61$
$4.0 < y < 4.5$	$5103 \pm 73 \pm 90$	$1596 \pm 50 \pm 42$

C Nuclear modification factor

Tables 12 and 13 list the nuclear modification factors $R_{p\text{Pb}}^{\Upsilon(1S)}$ for $\Upsilon(1S)$ in transverse momentum bins and in rapidity bins. Tables 14 and 15 listed the nuclear modification factors for $\Upsilon(1S)$ $R_{p\text{Pb}}^{\Upsilon(2S)}$ for $\Upsilon(2S)$ in transverse momentum bins and in rapidity bins. In all tables, the quoted uncertainties are the sum in quadrature of the statistical and systematic components.

Table 12: $\Upsilon(1S)$ nuclear modification factor, $R_{p\text{Pb}}^{\Upsilon(1S)}$, in $p\text{Pb}$ and Pbp as a function of p_{T} integrated over y^* in the range $1.5 < y^* < 4.0$ for $p\text{Pb}$ and $-5.0 < y^* < -2.5$ for Pbp .

p_{T} [GeV/c]	$R_{p\text{Pb}}^{\Upsilon(1S)}$ in $p\text{Pb}$	$R_{p\text{Pb}}^{\Upsilon(1S)}$ in Pbp
$0 < p_{\text{T}} < 2$	0.46 ± 0.06	0.76 ± 0.11
$2 < p_{\text{T}} < 4$	0.46 ± 0.05	0.92 ± 0.13
$4 < p_{\text{T}} < 6$	0.66 ± 0.07	0.90 ± 0.13
$6 < p_{\text{T}} < 8$	0.67 ± 0.08	0.91 ± 0.17
$8 < p_{\text{T}} < 10$	0.79 ± 0.10	0.81 ± 0.12
$10 < p_{\text{T}} < 15$	0.84 ± 0.10	1.14 ± 0.16
$15 < p_{\text{T}} < 25$	0.87 ± 0.16	1.04 ± 0.18

Table 13: $\Upsilon(1S)$ nuclear modification factor, $R_{p\text{Pb}}^{\Upsilon(1S)}$, in $p\text{Pb}$ and Pbp as a function of y^* integrated over p_{T} in the range $0 < p_{\text{T}} < 25$ GeV/c.

y^*	$R_{p\text{Pb}}^{\Upsilon(1S)}$
$-4.5 < y^* < -4.0$	1.09 ± 0.14
$-4.0 < y^* < -3.5$	0.82 ± 0.12
$-3.5 < y^* < -3.0$	0.88 ± 0.12
$-3.0 < y^* < -2.5$	1.09 ± 0.13
$2.0 < y^* < 2.5$	0.67 ± 0.06
$2.5 < y^* < 3.0$	0.64 ± 0.06
$3.0 < y^* < 3.5$	0.60 ± 0.07
$3.5 < y^* < 4.0$	0.66 ± 0.10

Table 14: $\Upsilon(2S)$ nuclear modification factor, $R_{p\text{Pb}}^{\Upsilon(2S)}$, in $p\text{Pb}$ and Pbp as a function of p_{T} integrated over y^* in the range $1.5 < y^* < 4.0$ for $p\text{Pb}$ and $-5.0 < y^* < -2.5$ for Pbp .

p_{T} [GeV/c]	$R_{p\text{Pb}}^{\Upsilon(2S)}$ in $p\text{Pb}$	$R_{p\text{Pb}}^{\Upsilon(2S)}$ in Pbp
$0 < p_{\text{T}} < 2$	0.22 ± 0.08	0.54 ± 0.17
$2 < p_{\text{T}} < 4$	0.38 ± 0.10	0.55 ± 0.11
$4 < p_{\text{T}} < 6$	0.35 ± 0.09	0.88 ± 0.17
$6 < p_{\text{T}} < 8$	0.30 ± 0.11	0.73 ± 0.31
$8 < p_{\text{T}} < 10$	0.49 ± 0.11	0.48 ± 0.15
$10 < p_{\text{T}} < 15$	0.69 ± 0.12	0.78 ± 0.18
$15 < p_{\text{T}} < 25$	0.78 ± 0.22	0.86 ± 0.35

Table 15: $\Upsilon(2S)$ nuclear modification factor, $R_{p\text{Pb}}^{\Upsilon(2S)}$, in $p\text{Pb}$ and Pbp as a function of y^* integrated over p_{T} in the range $0 < p_{\text{T}} < 25$ GeV/c.

y^*	$R_{p\text{Pb}}^{\Upsilon(2S)}$
$-4.5 < y^* < -4.0$	0.61 ± 0.13
$-4.0 < y^* < -3.5$	0.83 ± 0.16
$-3.5 < y^* < -3.0$	0.72 ± 0.13
$-3.0 < y^* < -2.5$	0.76 ± 0.15
$2.0 < y^* < 2.5$	0.63 ± 0.11
$2.5 < y^* < 3.0$	0.61 ± 0.11
$3.0 < y^* < 3.5$	0.36 ± 0.10
$3.5 < y^* < 4.0$	0.46 ± 0.14

D Forward-to-backward ratios

Tables 16 and 17 list the forward-to-backward ratios $R_{\text{FB}}^{\Upsilon(1S)}$ for $\Upsilon(1S)$ in transverse momentum bins and in rapidity bins. In all tables, the quoted uncertainties are the sum in quadrature of the statistical and systematic components. The ratio $R_{\text{FB}}^{\Upsilon(2S)}$ integrated over $|y^*|$ in the range $2.5 < |y^*| < 4.0$, and over p_T in the range $0 < p_T < 25$ GeV/ c is 0.66 ± 0.23 .

Table 16: $\Upsilon(1S)$ forward-to-backward ratio, $R_{\text{FB}}^{\Upsilon(1S)}$, as a function of p_T integrated over $|y^*|$ in the range $2.5 < |y^*| < 4.0$.

p_T [GeV/ c]	$R_{\text{FB}}^{\Upsilon(1S)}$
$0 < p_T < 2$	0.73 ± 0.19
$2 < p_T < 4$	0.74 ± 0.18
$4 < p_T < 6$	0.92 ± 0.19
$6 < p_T < 8$	1.01 ± 0.19
$8 < p_T < 10$	1.37 ± 0.20
$10 < p_T < 15$	1.22 ± 0.20
$15 < p_T < 25$	1.46 ± 0.26

Table 17: $\Upsilon(1S)$ forward-to-backward ratio, $R_{\text{FB}}^{\Upsilon(1S)}$, as a function of $|y^*|$ integrated over p_T in the range $0 < p_T < 25$ GeV/ c .

$ y^* $	$R_{\text{FB}}^{\Upsilon(1S)}$
$2.5 < y^* < 3.0$	0.59 ± 0.16
$3.0 < y^* < 3.5$	0.68 ± 0.18
$3.5 < y^* < 4.0$	0.80 ± 0.21

E Ratios between excited states

Tables 18 and 19 list the $\Upsilon(2S)$ to $\Upsilon(1S)$ ratios in bins of transverse momentum bins and rapidity. In all tables, the quoted uncertainties are the sum in quadrature of the statistical and systematic components.

Table 18: $\Upsilon(2S)$ to $\Upsilon(1S)$ ratio, $R(\Upsilon(2S))$, in $p\text{Pb}$ and Pbp as a function of p_{T} integrated over y^* in the range $1.5 < y^* < 4.0$ for $p\text{Pb}$ and $-5.0 < y^* < -2.5$ for Pbp .

p_{T} [GeV/c]	$R(\Upsilon(2S))$ in $p\text{Pb}$	$R(\Upsilon(2S))$ in Pbp
$0 < p_{\text{T}} < 2$	0.20 ± 0.06	0.21 ± 0.07
$2 < p_{\text{T}} < 4$	0.36 ± 0.06	0.25 ± 0.06
$4 < p_{\text{T}} < 6$	0.22 ± 0.05	0.33 ± 0.08
$6 < p_{\text{T}} < 8$	0.26 ± 0.06	0.29 ± 0.09
$8 < p_{\text{T}} < 10$	0.35 ± 0.07	0.28 ± 0.11
$10 < p_{\text{T}} < 15$	0.42 ± 0.08	0.41 ± 0.09
$15 < p_{\text{T}} < 25$	0.55 ± 0.15	0.49 ± 0.19

Table 19: $\Upsilon(2S)$ to $\Upsilon(1S)$ ratio, $R(\Upsilon(2S))$, in $p\text{Pb}$ and Pbp as a function of y^* integrated over p_{T} in the range $0 < p_{\text{T}} < 25$ GeV/c.

y^*	$R(2S)$
$-5.0 < y^* < -4.5$	0.27 ± 0.05
$-4.5 < y^* < -4.0$	0.18 ± 0.03
$-4.0 < y^* < -3.5$	0.34 ± 0.06
$-3.5 < y^* < -3.0$	0.28 ± 0.05
$-3.0 < y^* < -2.5$	0.24 ± 0.09
$1.5 < y^* < 2.0$	0.38 ± 0.08
$2.0 < y^* < 2.5$	0.31 ± 0.05
$2.5 < y^* < 3.0$	0.31 ± 0.05
$3.0 < y^* < 3.5$	0.19 ± 0.05
$3.5 < y^* < 4.0$	0.23 ± 0.07

F $\Upsilon(1S)$ to nonprompt J/ψ ratios

Table 20 lists the $\Upsilon(1S)$ to nonprompt J/ψ ratios in rapidity bins.

Table 20: $\Upsilon(1S)$ to nonprompt J/ψ , in $p\text{Pb}$ and Pbp as a function of y^* integrated over p_T in the range $0 < p_T < 25$ GeV/c. The quoted uncertainties are the sum in quadrature of the statistical and systematic components.

y^*	$\Upsilon(1S)$ to J/ψ -from-b
$-5.0 < y^* < -4.5$	0.125 ± 0.020
$-4.5 < y^* < -4.0$	0.102 ± 0.013
$-4.0 < y^* < -3.5$	0.087 ± 0.013
$-3.5 < y^* < -3.0$	0.094 ± 0.013
$-3.0 < y^* < -2.5$	0.112 ± 0.014
$1.5 < y^* < 2.0$	0.077 ± 0.008
$2.0 < y^* < 2.5$	0.074 ± 0.007
$2.5 < y^* < 3.0$	0.082 ± 0.008
$3.0 < y^* < 3.5$	0.078 ± 0.009
$3.5 < y^* < 4.0$	0.091 ± 0.013

References

- [1] STAR collaboration, J. Adams *et al.*, *Experimental and theoretical challenges in the search for the quark-gluon plasma: The STAR Collaboration's critical assessment of the evidence from RHIC collisions*, Nucl. Phys. **A757** (2005) 102, [arXiv:nucl-ex/0501009](https://arxiv.org/abs/nucl-ex/0501009).
- [2] R. Maciula and A. Szczerba, *Open charm production at the LHC: k_t -factorization approach*, Phys. Rev. **D87** (2013) 094022, [arXiv:1301.3033](https://arxiv.org/abs/1301.3033).
- [3] T. Matsui and H. Satz, *J/ψ suppression by quark-gluon plasma formation*, Phys. Lett. **B178** (1986) 416.
- [4] D. de Florian, R. Sassot, P. Zurita, and M. Stratmann, *Global Analysis of Nuclear Parton Distributions*, Phys. Rev. **D85** (2012) 074028, [arXiv:1112.6324](https://arxiv.org/abs/1112.6324).
- [5] J. F. Owens, A. Accardi, and W. Melnitchouk, *Global parton distributions with nuclear and finite- Q^2 corrections*, Phys. Rev. **D87** (2013) 094012, [arXiv:1212.1702](https://arxiv.org/abs/1212.1702).
- [6] K. J. Eskola, H. Paukkunen, and C. A. Salgado, *EPS09: A New Generation of NLO and LO Nuclear Parton Distribution Functions*, JHEP **04** (2009) 065, [arXiv:0902.4154](https://arxiv.org/abs/0902.4154).
- [7] K. Kovarik *et al.*, *nCTEQ15 - Global analysis of nuclear parton distributions with uncertainties in the CTEQ framework*, Phys. Rev. **D93** (2016) 085037, [arXiv:1509.00792](https://arxiv.org/abs/1509.00792).
- [8] F. Arleo and S. Peigné, *Quarkonium suppression in heavy-ion collisions from coherent energy loss in cold nuclear matter*, JHEP **10** (2014) 073, [arXiv:1407.5054](https://arxiv.org/abs/1407.5054).
- [9] F. Arleo, R. Kolevatov, S. Peigné, and M. Rustamova, *Centrality and p_\perp dependence of J/ψ suppression in proton-nucleus collisions from parton energy loss*, JHEP **05** (2013) 155, [arXiv:1304.0901](https://arxiv.org/abs/1304.0901).
- [10] F. Arleo and S. Peigné, *Heavy-quarkonium suppression in p - A collisions from parton energy loss in cold QCD matter*, JHEP **03** (2013) 122, [arXiv:1212.0434](https://arxiv.org/abs/1212.0434).
- [11] C. Gerschel and J. Hüfner, *A contribution to the suppression of the J/ψ meson produced in high-energy nucleus-nucleus collisions*, Phys. Lett. **B207** (1988) 253.
- [12] J. L. Albacete *et al.*, *Predictions for p + Pb collisions at $\sqrt{s_{NN}} = 5$ TeV*, Int. J. Mod. Phys. **E22** (2013) 1330007, [arXiv:1301.3395](https://arxiv.org/abs/1301.3395).
- [13] A. Adeluyi and T. Nguyen, *Coherent photoproduction of ψ and Υ mesons in ultraperipheral p Pb and PbPb collisions at the CERN Large Hadron Collider at $\sqrt{s_{NN}} = 5$ TeV and $\sqrt{s_{NN}} = 2.76$ TeV*, Phys. Rev. **C87** (2013) 027901, [arXiv:1302.4288](https://arxiv.org/abs/1302.4288).
- [14] G. A. Chirilli, B.-W. Xiao, and F. Yuan, *Inclusive hadron productions in p A collisions*, Phys. Rev. **D86** (2012) 054005, [arXiv:1203.6139](https://arxiv.org/abs/1203.6139).

- [15] G. A. Chirilli, *High-Energy QCD factorization from DIS to pA collisions*, Int. J. Mod. Phys. Conf. Ser. **20** (2012) 200, [arXiv:1209.1614](#).
- [16] E. G. Ferreiro, F. Fleuret, J. P. Lansberg, and A. Rakotozafindrabe, *Impact of the nuclear modification of the gluon densities on J/ψ production in pPb collisions at $\sqrt{s_{NN}} = 5$ TeV*, Phys. Rev. **C88** (2013) 047901, [arXiv:1305.4569](#).
- [17] E. G. Ferreiro and J.-P. Lansberg, *Is bottomonium suppression in proton-nucleus and nucleus-nucleus collisions at LHC energies due to the same effects?*, [arXiv:1804.04474](#).
- [18] E. G. Ferreiro, *Excited charmonium suppression in proton–nucleus collisions as a consequence of comovers*, Phys. Lett. **B749** (2015) 98, [arXiv:1411.0549](#).
- [19] X. Du and R. Rapp, *Sequential Regeneration of Charmonia in Heavy-Ion Collisions*, Nucl. Phys. **A943** (2015) 147, [arXiv:1504.00670](#).
- [20] Y.-Q. Ma, R. Venugopalan, K. Watanabe, and H.-F. Zhang, $\psi(2S)$ versus J/ψ suppression in proton–nucleus collisions from factorization violating soft color exchanges, Phys. Rev. **C97** (2018) 014909, [arXiv:1707.07266](#).
- [21] CMS collaboration, S. Chatrchyan *et al.*, *Indications of suppression of excited Υ states in $PbPb$ collisions at $\sqrt{S_{NN}} = 2.76$ TeV*, Phys. Rev. Lett. **107** (2011) 052302, [arXiv:1105.4894](#).
- [22] ATLAS, M. Aaboud *et al.*, *Measurement of quarkonium production in proton–lead and proton–proton collisions at 5.02 TeV with the ATLAS detector*, Eur. Phys. J. **C78** (2018) 171, [arXiv:1709.03089](#).
- [23] Z. Ye, Υ measurements in $p+p$, $p+Au$ and $Au+Au$ collisions at $\sqrt{s_{NN}} = 200$ GeV with the STAR experiment, Nucl. Phys. **A967** (2017) 600.
- [24] CMS collaboration, V. Khachatryan *et al.*, *Suppression of $\Upsilon(1S)$, $\Upsilon(2S)$ and $\Upsilon(3S)$ quarkonium states in $PbPb$ collisions at $\sqrt{s_{NN}} = 2.76$ TeV*, Phys. Lett. **B770** (2017) 357, [arXiv:1611.01510](#).
- [25] CMS collaboration, S. Chatrchyan *et al.*, *Event activity dependence of $\Upsilon(nS)$ production in $\sqrt{s_{NN}} = 5.02$ TeV pPb and $\sqrt{s}=2.76$ TeV pp collisions*, JHEP **04** (2014) 103, [arXiv:1312.6300](#).
- [26] CMS collaboration, A. M. Sirunyan *et al.*, *Suppression of excited Υ states relative to the ground state in $Pb-Pb$ collisions at $\sqrt{s_{NN}} = 5.02$ TeV*, Phys. Rev. Lett. **120** (2018) 142301, [arXiv:1706.05984](#).
- [27] ALICE collaboration, B. B. Abelev *et al.*, *Production of inclusive $\Upsilon(1S)$ and $\Upsilon(2S)$ in $p-Pb$ collisions at $\sqrt{s_{NN}} = 5.02$ TeV*, Phys. Lett. **B740** (2015) 105, [arXiv:1410.2234](#).
- [28] LHCb collaboration, R. Aaij *et al.*, *Study of Υ production and cold nuclear matter effects in pPb collisions at $\sqrt{s_{NN}} = 5$ TeV*, JHEP **07** (2014) 094, [arXiv:1405.5152](#).

- [29] LHCb collaboration, R. Aaij *et al.*, *Prompt and nonprompt J/ψ production and nuclear modification in pPb collisions at $\sqrt{s_{NN}} = 8.16 \text{ TeV}$* , Phys. Lett. **B774** (2017) 159, [arXiv:1706.07122](#).
- [30] LHCb collaboration, A. A. Alves Jr. *et al.*, *The LHCb detector at the LHC*, JINST **3** (2008) S08005.
- [31] LHCb collaboration, R. Aaij *et al.*, *LHCb detector performance*, Int. J. Mod. Phys. **A30** (2015) 1530022, [arXiv:1412.6352](#).
- [32] R. Aaij *et al.*, *Performance of the LHCb Vertex Locator*, JINST **9** (2014) P09007, [arXiv:1405.7808](#).
- [33] R. Arink *et al.*, *Performance of the LHCb Outer Tracker*, JINST **9** (2014) P01002, [arXiv:1311.3893](#).
- [34] M. Adinolfi *et al.*, *Performance of the LHCb RICH detector at the LHC*, Eur. Phys. J. **C73** (2013) 2431, [arXiv:1211.6759](#).
- [35] A. A. Alves Jr. *et al.*, *Performance of the LHCb muon system*, JINST **8** (2013) P02022, [arXiv:1211.1346](#).
- [36] R. Aaij *et al.*, *The LHCb trigger and its performance in 2011*, JINST **8** (2013) P04022, [arXiv:1211.3055](#).
- [37] G. Dujany and B. Storaci, *Real-time alignment and calibration of the LHCb Detector in Run II*, J. Phys. Conf. Ser. **664** (2015) 082010.
- [38] R. Aaij *et al.*, *Tesla: an application for real-time data analysis in High Energy Physics*, Comput. Phys. Commun. **208** (2016) 35, [arXiv:1604.05596](#).
- [39] LHCb collaboration, R. Aaij *et al.*, *Study of J/ψ production in jets*, Phys. Rev. Lett. **118** (2017) 192001, [arXiv:1701.05116](#).
- [40] T. Pierog *et al.*, *EPOS LHC: Test of collective hadronization with data measured at the CERN Large Hadron Collider*, Phys. Rev. **C92** (2015) 034906, [arXiv:1306.0121](#).
- [41] T. Sjöstrand, S. Mrenna, and P. Skands, *PYTHIA 6.4 physics and manual*, JHEP **05** (2006) 026, [arXiv:hep-ph/0603175](#); T. Sjöstrand, S. Mrenna, and P. Skands, *A brief introduction to PYTHIA 8.1*, Comput. Phys. Commun. **178** (2008) 852, [arXiv:0710.3820](#).
- [42] Geant4 collaboration, J. Allison *et al.*, *Geant4 developments and applications*, IEEE Trans. Nucl. Sci. **53** (2006) 270; Geant4 collaboration, S. Agostinelli *et al.*, *Geant4: A simulation toolkit*, Nucl. Instrum. Meth. **A506** (2003) 250.
- [43] M. Clemencic *et al.*, *The LHCb simulation application, Gauss: Design, evolution and experience*, J. Phys. Conf. Ser. **331** (2011) 032023.
- [44] LHCb collaboration, R. Aaij *et al.*, *Measurement of the Υ polarizations in pp collisions at $\sqrt{s_{NN}} = 7$ and 8 TeV* , JHEP **12** (2017) 110, [arXiv:1709.01301](#).

- [45] LHCb collaboration, R. Aaij *et al.*, *Precision luminosity measurements at LHCb*, JINST **9** (2014) P12005, [arXiv:1410.0149](#).
- [46] Particle Data Group, M. Tanabashi *et al.*, *Review of particle physics*, Phys. Rev. D **98** (2018) 030001.
- [47] T. Skwarnicki, *A study of the radiative cascade transitions between the Upsilon-prime and Upsilon resonances*, PhD thesis, Institute of Nuclear Physics, Krakow, 1986, DESY-F31-86-02.
- [48] LHCb collaboration, R. Aaij *et al.*, *Measurement of Υ production in pp collisions at $\sqrt{s} = 2.76 \text{ TeV}$* , Eur. Phys. J. **C74** (2014) 2835, [arXiv:1402.2539](#).
- [49] LHCb collaboration, R. Aaij *et al.*, *Forward production of Υ mesons in pp collisions at $\sqrt{s} = 7$ and 8 TeV*, JHEP **11** (2015) 103, [arXiv:1509.02372](#).
- [50] LHCb collaboration, R. Aaij *et al.*, *Measurement of Υ production cross-section in pp collisions at $\sqrt{s} = 13 \text{ TeV}$* , JHEP **07** (2018) 134, [arXiv:1804.09214](#).
- [51] J.-P. Lansberg and H.-S. Shao, *Towards an automated tool to evaluate the impact of the nuclear modification of the gluon density on quarkonium, D and B meson production in proton–nucleus collisions*, Eur. Phys. J. **C77** (2017) 1, [arXiv:1610.05382](#).
- [52] H.-S. Shao, *HELAC-Onia 2.0: An upgraded matrix-element and event generator for heavy quarkonium physics*, Comput. Phys. Commun. **198** (2016) 238, [arXiv:1507.03435](#).
- [53] H.-S. Shao, *HELAC-Onia: An automatic matrix element generator for heavy quarkonium physics*, Comput. Phys. Commun. **184** (2013) 2562, [arXiv:1212.5293](#).
- [54] K. J. Eskola, P. Paakkinen, H. Paukkunen, and C. A. Salgado, *EPPS16 - Bringing nuclear PDFs to the LHC era*, in *12th International Workshop on High-pT Physics in the RHIC/LHC Era (HPT 2017) Bergen, Norway, October 2-5, 2017*, 2018. [arXiv:1802.00713](#).
- [55] X. Yao and B. Müller, *Approach to equilibrium of quarkonium in quark-gluon plasma*, Phys. Rev. C **97** (2018) 014908, [arXiv:1709.03539](#).
- [56] M. Winn, *Prospects for quarkonium measurements in p-A and A-A collisions at the LHC*, Few Body Syst. **58** (2017) 53, [arXiv:1609.01135](#).

LHCb collaboration

R. Aaij²⁸, C. Abellán Beteta⁴⁵, B. Adeva⁴², M. Adinolfi⁴⁹, C.A. Aidala⁷⁶, Z. Ajaltouni⁶, S. Akar⁶⁰, P. Albicocco¹⁹, J. Albrecht¹¹, F. Alessio⁴³, M. Alexander⁵⁴, A. Alfonso Albero⁴¹, G. Alkhazov³⁴, P. Alvarez Cartelle⁵⁶, A.A. Alves Jr⁴², S. Amato², S. Amerio²⁴, Y. Amhis⁸, L. An³, L. Anderlini¹⁸, G. Andreassi⁴⁴, M. Andreotti¹⁷, J.E. Andrews⁶¹, R.B. Appleby⁵⁷, F. Archilli²⁸, P. d'Argent¹³, J. Arnau Romeu⁷, A. Artamonov⁴⁰, M. Artuso⁶², K. Arzymatow³⁸, E. Aslanides⁷, M. Atzeni⁴⁵, B. Audurier²³, S. Bachmann¹³, J.J. Back⁵¹, S. Baker⁵⁶, V. Balagura^{8,b}, W. Baldini¹⁷, A. Baranov³⁸, R.J. Barlow⁵⁷, S. Barsuk⁸, W. Barter⁵⁷, M. Bartolini²⁰, F. Baryshnikov⁷³, V. Batozskaya³², B. Batsukh⁶², A. Battig¹¹, V. Battista⁴⁴, A. Bay⁴⁴, J. Beddow⁵⁴, F. Bedeschi²⁵, I. Bediaga¹, A. Beiter⁶², L.J. Bel²⁸, S. Belin²³, N. Belyi⁶⁵, V. Bellee⁴⁴, N. Belloli^{21,i}, K. Belous⁴⁰, I. Belyaev³⁵, E. Ben-Haim⁹, G. Bencivenni¹⁹, S. Benson²⁸, S. Beranek¹⁰, A. Berezhnoy³⁶, R. Bernet⁴⁵, D. Berninghoff¹³, E. Bertholet⁹, A. Bertolin²⁴, C. Betancourt⁴⁵, F. Betti^{16,43}, M.O. Bettler⁵⁰, M. van Beuzekom²⁸, Ia. Bezshyiko⁴⁵, S. Bhasin⁴⁹, J. Bhom³⁰, S. Bifani⁴⁸, P. Billoir⁹, A. Birnkraut¹¹, A. Bizzeti^{18,u}, M. Bjørn⁵⁸, M.P. Blago⁴³, T. Blake⁵¹, F. Blanc⁴⁴, S. Blusk⁶², D. Bobulska⁵⁴, V. Bocci²⁷, O. Boente Garcia⁴², T. Boettcher⁵⁹, A. Bondar^{39,w}, N. Bondar³⁴, S. Borghi^{57,43}, M. Borisjak³⁸, M. Borsato⁴², F. Bossu⁸, M. Boubdir¹⁰, T.J.V. Bowcock⁵⁵, C. Bozzi^{17,43}, S. Braun¹³, M. Brodski⁴³, J. Brodzicka³⁰, A. Brossa Gonzalo⁵¹, D. Brundu^{23,43}, E. Buchanan⁴⁹, A. Buonaura⁴⁵, C. Burr⁵⁷, A. Bursche²³, J. Buytaert⁴³, W. Byczynski⁴³, S. Cadeddu²³, H. Cai⁶⁷, R. Calabrese^{17,g}, R. Calladine⁴⁸, M. Calvi^{21,i}, M. Calvo Gomez^{41,m}, A. Camboni^{41,m}, P. Campana¹⁹, D.H. Campora Perez⁴³, L. Capriotti¹⁶, A. Carbone^{16,e}, G. Carboni²⁶, R. Cardinale²⁰, A. Cardini²³, P. Carniti^{21,i}, L. Carson⁵³, K. Carvalho Akiba², G. Casse⁵⁵, L. Cassina²¹, M. Cattaneo⁴³, G. Cavallero^{20,h}, R. Cenci^{25,p}, D. Chamont⁸, M.G. Chapman⁴⁹, M. Charles⁹, Ph. Charpentier⁴³, G. Chatzikonstantinidis⁴⁸, M. Chefdeville⁵, V. Chekalina³⁸, C. Chen³, S. Chen²³, S.-G. Chitic⁴³, V. Chobanova⁴², M. Chrzaszcz⁴³, A. Chubykin³⁴, P. Ciambrone¹⁹, X. Cid Vidal⁴², G. Ciezarek⁴³, P.E.L. Clarke⁵³, M. Clemencic⁴³, H.V. Cliff⁵⁰, J. Closier⁴³, V. Coco⁴³, J.A.B. Coelho⁸, J. Cogan⁷, E. Cogneras⁶, L. Cojocariu³³, P. Collins⁴³, T. Colombo⁴³, A. Comerma-Montells¹³, A. Contu²³, G. Coombs⁴³, S. Coquereau⁴¹, G. Corti⁴³, M. Corvo^{17,g}, C.M. Costa Sobral⁵¹, B. Couturier⁴³, G.A. Cowan⁵³, D.C. Craik⁵⁹, A. Crocombe⁵¹, M. Cruz Torres¹, R. Currie⁵³, C. D'Ambrosio⁴³, F. Da Cunha Marinho², C.L. Da Silva⁷⁷, E. Dall'Occo²⁸, J. Dalseno⁴⁹, A. Danilina³⁵, A. Davis³, O. De Aguiar Francisco⁴³, K. De Bruyn⁴³, S. De Capua⁵⁷, M. De Cian⁴⁴, J.M. De Miranda¹, L. De Paula², M. De Serio^{15,d}, P. De Simone¹⁹, C.T. Dean⁵⁴, D. Decamp⁵, L. Del Buono⁹, B. Delaney⁵⁰, H.-P. Dembinski¹², M. Demmer¹¹, A. Dendek³¹, D. Derkach³⁸, O. Deschamps⁶, F. Desse⁸, F. Dettori⁵⁵, B. Dey⁶⁸, A. Di Canto⁴³, P. Di Nezza¹⁹, S. Didenko⁷³, H. Dijkstra⁴³, F. Dordei⁴³, M. Dorigo^{43,y}, A. Dosil Suárez⁴², L. Douglas⁵⁴, A. Dovbnya⁴⁶, K. Dreimanis⁵⁵, L. Dufour²⁸, G. Dujany⁹, P. Durante⁴³, J.M. Durham⁷⁷, D. Dutta⁵⁷, R. Dzhelyadin⁴⁰, M. Dziewiecki¹³, A. Dziurda³⁰, A. Dzyuba³⁴, S. Easo⁵², U. Egede⁵⁶, V. Egorychev³⁵, S. Eidelman^{39,w}, S. Eisenhardt⁵³, U. Eitschberger¹¹, R. Ekelhof¹¹, L. Eklund⁵⁴, S. Ely⁶², A. Ene³³, S. Escher¹⁰, S. Esen²⁸, T. Evans⁶⁰, A. Falabella¹⁶, N. Farley⁴⁸, S. Farry⁵⁵, D. Fazzini^{21,43,i}, L. Federici²⁶, P. Fernandez Declara⁴³, A. Fernandez Prieto⁴², F. Ferrari¹⁶, L. Ferreira Lopes⁴⁴, F. Ferreira Rodrigues², M. Ferro-Luzzi⁴³, S. Filippov³⁷, R.A. Fini¹⁵, M. Fiorini^{17,g}, M. Firlej³¹, C. Fitzpatrick⁴⁴, T. Fiutowski³¹, F. Fleuret^{8,b}, M. Fontana⁴³, F. Fontanelli^{20,h}, R. Forty⁴³, V. Franco Lima⁵⁵, M. Frank⁴³, C. Frei⁴³, J. Fu^{22,q}, W. Funk⁴³, C. Färber⁴³, M. Féo Pereira Rivello Carvalho²⁸, E. Gabriel⁵³, A. Gallas Torreira⁴², D. Galli^{16,e}, S. Gallorini²⁴, S. Gambetta⁵³, Y. Gan³, M. Gandelman², P. Gandini²², Y. Gao³, L.M. Garcia Martin⁷⁵, B. Garcia Plana⁴², J. García Pardiñas⁴⁵, J. Garra Tico⁵⁰, L. Garrido⁴¹, D. Gascon⁴¹, C. Gaspar⁴³, L. Gavardi¹¹, G. Gazzoni⁶, D. Gerick¹³, E. Gersabeck⁵⁷, M. Gersabeck⁵⁷, T. Gershon⁵¹, D. Gerstel⁷, Ph. Ghez⁵, V. Gibson⁵⁰, O.G. Girard⁴⁴,

P. Gironella Gironell⁴¹, L. Giubega³³, K. Gizdov⁵³, V.V. Gligorov⁹, D. Golubkov³⁵,
 A. Golutvin^{56,73}, A. Gomes^{1,a}, I.V. Gorelov³⁶, C. Gotti^{21,i}, E. Govorkova²⁸, J.P. Grabowski¹³,
 R. Graciani Diaz⁴¹, L.A. Granado Cardoso⁴³, E. Graugés⁴¹, E. Graverini⁴⁵, G. Graziani¹⁸,
 A. Grecu³³, R. Greim²⁸, P. Griffith²³, L. Grillo⁵⁷, L. Gruber⁴³, B.R. Gruberg Cazon⁵⁸,
 O. Grünberg⁷⁰, C. Gu³, E. Gushchin³⁷, A. Guth¹⁰, Yu. Guz^{40,43}, T. Gys⁴³, C. Göbel⁶⁴,
 T. Hadavizadeh⁵⁸, C. Hadjivasiliou⁶, G. Haefeli⁴⁴, C. Haen⁴³, S.C. Haines⁵⁰, B. Hamilton⁶¹,
 X. Han¹³, T.H. Hancock⁵⁸, S. Hansmann-Menzemer¹³, N. Harnew⁵⁸, S.T. Harnew⁴⁹,
 T. Harrison⁵⁵, C. Hasse⁴³, M. Hatch⁴³, J. He⁶⁵, M. Hecker⁵⁶, K. Heinicke¹¹, A. Heister¹¹,
 K. Hennessy⁵⁵, L. Henry⁷⁵, E. van Herwijnen⁴³, J. Heuel¹⁰, M. Heß⁷⁰, A. Hicheur⁶³,
 R. Hidalgo Charman⁵⁷, D. Hill⁵⁸, M. Hilton⁵⁷, P.H. Hopchev⁴⁴, J. Hu¹³, W. Hu⁶⁸, W. Huang⁶⁵,
 Z.C. Huard⁶⁰, W. Hulsbergen²⁸, T. Humair⁵⁶, M. Hushchyn³⁸, D. Hutchcroft⁵⁵, D. Hynds²⁸,
 P. Ibis¹¹, M. Idzik³¹, P. Ilten⁴⁸, K. Ivshin³⁴, R. Jacobsson⁴³, J. Jalocha⁵⁸, E. Jans²⁸,
 A. Jawahery⁶¹, F. Jiang³, M. John⁵⁸, D. Johnson⁴³, C.R. Jones⁵⁰, C. Joram⁴³, B. Jost⁴³,
 N. Jurik⁵⁸, S. Kandybei⁴⁶, M. Karacson⁴³, J.M. Kariuki⁴⁹, S. Karodia⁵⁴, N. Kazeev³⁸,
 M. Kecke¹³, F. Keizer⁵⁰, M. Kelsey⁶², M. Kenzie⁵⁰, T. Ketel²⁹, E. Khairullin³⁸, B. Khanji⁴³,
 C. Khurewathanakul⁴⁴, K.E. Kim⁶², T. Kirn¹⁰, S. Klaver¹⁹, K. Klimaszewski³²,
 T. Klimkovich¹², S. Koliev⁴⁷, M. Kolpin¹³, R. Kopecna¹³, P. Koppenburg²⁸, I. Kostiuuk²⁸,
 S. Kotriakhova³⁴, M. Kozeiha⁶, L. Kravchuk³⁷, M. Kreps⁵¹, F. Kress⁵⁶, P. Krokovny^{39,w},
 W. Krupa³¹, W. Krzemien³², W. Kucewicz^{30,l}, M. Kucharczyk³⁰, V. Kudryavtsev^{39,w},
 A.K. Kuonen⁴⁴, T. Kvaratskheliya^{35,43}, D. Lacarrere⁴³, G. Lafferty⁵⁷, A. Lai²³, D. Lancierini⁴⁵,
 G. Lanfranchi¹⁹, C. Langenbruch¹⁰, T. Latham⁵¹, C. Lazzeroni⁴⁸, R. Le Gac⁷, A. Leflat³⁶,
 J. Lefrançois⁸, R. Lefèvre⁶, F. Lemaitre⁴³, O. Leroy⁷, T. Lesiak³⁰, B. Leverington¹³, P.-R. Li⁶⁵,
 Y. Li⁴, Z. Li⁶², X. Liang⁶², T. Likhomannenko⁷², R. Lindner⁴³, F. Lionetto⁴⁵, V. Lisovskyi⁸,
 G. Liu⁶⁶, X. Liu³, D. Loh⁵¹, A. Loi²³, I. Longstaff⁵⁴, J.H. Lopes², G.H. Lovell⁵⁰, D. Lucchesi^{24,o},
 M. Lucio Martinez⁴², A. Lupato²⁴, E. Luppi^{17,g}, O. Lupton⁴³, A. Lusiani²⁵, X. Lyu⁶⁵,
 F. Machefert⁸, F. Maciuc³³, V. Macko⁴⁴, P. Mackowiak¹¹, S. Maddrell-Mander⁴⁹, O. Maev^{34,43},
 K. Maguire⁵⁷, D. Maisuzenko³⁴, M.W. Majewski³¹, S. Malde⁵⁸, B. Malecki³⁰, A. Malinin⁷²,
 T. Maltsev^{39,w}, G. Manca^{23,f}, G. Mancinelli⁷, D. Marangotto^{22,q}, J. Maratas^{6,v},
 J.F. Marchand⁵, U. Marconi¹⁶, C. Marin Benito⁸, M. Marinangeli⁴⁴, P. Marino⁴⁴, J. Marks¹³,
 P.J. Marshall⁵⁵, G. Martellotti²⁷, M. Martin⁷, M. Martinelli⁴³, D. Martinez Santos⁴²,
 F. Martinez Vidal⁷⁵, A. Massafferri¹, M. Materok¹⁰, R. Matev⁴³, A. Mathad⁵¹, Z. Mathe⁴³,
 C. Matteuzzi²¹, A. Mauri⁴⁵, E. Maurice^{8,b}, B. Maurin⁴⁴, A. Mazurov⁴⁸, M. McCann^{56,43},
 A. McNab⁵⁷, R. McNulty¹⁴, J.V. Mead⁵⁵, B. Meadows⁶⁰, C. Meaux⁷, N. Meinert⁷⁰,
 D. Melnychuk³², M. Merk²⁸, A. Merli^{22,q}, E. Michelin²⁴, D.A. Milanes⁶⁹, E. Millard⁵¹,
 M.-N. Minard⁵, L. Minzoni^{17,g}, D.S. Mitzel¹³, A. Mogini⁹, R.D. Moise⁵⁶, T. Mombächer¹¹,
 I.A. Monroy⁶⁹, S. Monteil⁶, M. Morandin²⁴, G. Morello¹⁹, M.J. Morello^{25,t}, O. Morgunova⁷²,
 J. Moron³¹, A.B. Morris⁷, R. Mountain⁶², F. Muheim⁵³, M. Mulder²⁸, C.H. Murphy⁵⁸,
 D. Murray⁵⁷, A. Mödden¹¹, D. Müller⁴³, J. Müller¹¹, K. Müller⁴⁵, V. Müller¹¹, P. Naik⁴⁹,
 T. Nakada⁴⁴, R. Nandakumar⁵², A. Nandi⁵⁸, T. Nanut⁴⁴, I. Nasteva², M. Needham⁵³, N. Neri²²,
 S. Neubert¹³, N. Neufeld⁴³, M. Neuner¹³, R. Newcombe⁵⁶, T.D. Nguyen⁴⁴, C. Nguyen-Mau^{44,n},
 S. Nieswand¹⁰, R. Niet¹¹, N. Nikitin³⁶, A. Nogay⁷², N.S. Nolte⁴³, D.P. O'Hanlon¹⁶,
 A. Oblakowska-Mucha³¹, V. Obraztsov⁴⁰, S. Ogilvy¹⁹, R. Oldeman^{23,f}, C.J.G. Onderwater⁷¹,
 A. Ossowska³⁰, J.M. Otalora Goicochea², P. Owen⁴⁵, A. Oyanguren⁷⁵, P.R. Pais⁴⁴, T. Pajero^{25,t},
 A. Palano¹⁵, M. Palutan¹⁹, G. Panshin⁷⁴, A. Papanestis⁵², M. Pappagallo⁵³,
 L.L. Pappalardo^{17,g}, W. Parker⁶¹, C. Parkes^{57,43}, G. Passaleva^{18,43}, A. Pastore¹⁵, M. Patel⁵⁶,
 C. Patrignani^{16,e}, A. Pearce⁴³, A. Pellegrino²⁸, G. Penso²⁷, M. Pepe Altarelli⁴³, S. Perazzini⁴³,
 D. Pereima³⁵, P. Perret⁶, L. Pescatore⁴⁴, K. Petridis⁴⁹, A. Petrolini^{20,h}, A. Petrov⁷²,
 S. Petrucci⁵³, M. Petruzzo^{22,q}, B. Pietrzik⁵, G. Pietrzik⁴⁴, M. Pikies³⁰, M. Pili⁵⁸, D. Pinci²⁷,
 J. Pinzino⁴³, F. Pisani⁴³, A. Piucci¹³, V. Placinta³³, S. Playfer⁵³, J. Plews⁴⁸, M. Plo Casasus⁴²,
 F. Polci⁹, M. Poli Lener¹⁹, A. Poluektov⁵¹, N. Polukhina^{73,c}, I. Polyakov⁶², E. Polycarpo²,

G.J. Pomery⁴⁹, S. Ponce⁴³, A. Popov⁴⁰, D. Popov^{48,12}, S. Poslavskii⁴⁰, C. Potterat², E. Price⁴⁹,
 J. Prisciandaro⁴², C. Prouve⁴⁹, V. Pugatch⁴⁷, A. Puig Navarro⁴⁵, H. Pullen⁵⁸, G. Punzi^{25,p},
 W. Qian⁶⁵, J. Qin⁶⁵, R. Quagliani⁹, B. Quintana⁶, B. Rachwal³¹, J.H. Rademacker⁴⁹,
 M. Rama²⁵, M. Ramos Pernas⁴², M.S. Rangel², F. Ratnikov^{38,x}, G. Raven²⁹,
 M. Ravonel Salzgeber⁴³, M. Reboud⁵, F. Redi⁴⁴, S. Reichert¹¹, A.C. dos Reis¹, F. Reiss⁹,
 C. Remon Alepuz⁷⁵, Z. Ren³, V. Renaudin⁸, S. Ricciardi⁵², S. Richards⁴⁹, K. Rinnert⁵⁵,
 P. Robbe⁸, A. Robert⁹, A.B. Rodrigues⁴⁴, E. Rodrigues⁶⁰, J.A. Rodriguez Lopez⁶⁹,
 M. Roehrken⁴³, S. Roiser⁴³, A. Rollings⁵⁸, V. Romanovskiy⁴⁰, A. Romero Vidal⁴²,
 M. Rotondo¹⁹, M.S. Rudolph⁶², T. Ruf⁴³, J. Ruiz Vidal⁷⁵, J.J. Saborido Silva⁴², N. Sagidova³⁴,
 B. Saitta^{23,f}, V. Salustino Guimaraes⁶⁴, C. Sanchez Gras²⁸, C. Sanchez Mayordomo⁷⁵,
 B. Sanmartin Sedes⁴², R. Santacesaria²⁷, C. Santamarina Rios⁴², M. Santimaria^{19,43},
 E. Santovetti^{26,j}, G. Sarpis⁵⁷, A. Sarti^{19,k}, C. Satriano^{27,s}, A. Satta²⁶, M. Saur⁶⁵,
 D. Savrina^{35,36}, S. Schael¹⁰, M. Schellenberg¹¹, M. Schiller⁵⁴, H. Schindler⁴³, M. Schmelling¹²,
 T. Schmelzer¹¹, B. Schmidt⁴³, O. Schneider⁴⁴, A. Schopper⁴³, H.F. Schreiner⁶⁰, M. Schubiger⁴⁴,
 M.H. Schune⁸, R. Schwemmer⁴³, B. Sciascia¹⁹, A. Sciubba^{27,k}, A. Semennikov³⁵,
 E.S. Sepulveda⁹, A. Sergi^{48,43}, N. Serra⁴⁵, J. Serrano⁷, L. Sestini²⁴, A. Seuthe¹¹, P. Seyfert⁴³,
 M. Shapkin⁴⁰, Y. Shcheglov^{34,\dagger}, T. Shears⁵⁵, L. Shekhtman^{39,w}, V. Shevchenko⁷², E. Shmanin⁷³,
 B.G. Siddi¹⁷, R. Silva Coutinho⁴⁵, L. Silva de Oliveira², G. Simi^{24,o}, S. Simone^{15,d}, I. Skiba¹⁷,
 N. Skidmore¹³, T. Skwarnicki⁶², M.W. Slater⁴⁸, J.G. Smeaton⁵⁰, E. Smith¹⁰, I.T. Smith⁵³,
 M. Smith⁵⁶, M. Soares¹⁶, l. Soares Lavra¹, M.D. Sokoloff⁶⁰, F.J.P. Soler⁵⁴, B. Souza De Paula²,
 B. Spaan¹¹, E. Spadaro Norella^{22,q}, P. Spradlin⁵⁴, F. Stagni⁴³, M. Stahl¹³, S. Stahl⁴³,
 P. Steffko⁴⁴, S. Stefkova⁵⁶, O. Steinkamp⁴⁵, S. Stemmle¹³, O. Stenyakin⁴⁰, M. Stepanova³⁴,
 H. Stevens¹¹, A. Stocchi⁸, S. Stone⁶², B. Storaci⁴⁵, S. Stracka²⁵, M.E. Stramaglia⁴⁴,
 M. Straticiuc³³, U. Straumann⁴⁵, S. Strokov⁷⁴, J. Sun³, L. Sun⁶⁷, K. Swientek³¹, A. Szabelski³²,
 T. Szumlak³¹, M. Szymanski⁶⁵, S. T'Jampens⁵, Z. Tang³, A. Tayduganov⁷, T. Tekampe¹¹,
 G. Tellarini¹⁷, F. Teubert⁴³, E. Thomas⁴³, J. van Tilburg²⁸, M.J. Tilley⁵⁶, V. Tisserand⁶,
 M. Tobin³¹, S. Tolk⁴³, L. Tomassetti^{17,g}, D. Tonelli²⁵, D.Y. Tou⁹, R. Tourinho Jadallah Aoude¹,
 E. Tournefier⁵, M. Traill⁵⁴, M.T. Tran⁴⁴, A. Trisovic⁵⁰, A. Tsaregorodtsev⁷, G. Tuci^{25,p},
 A. Tully⁵⁰, N. Tuning^{28,43}, A. Ukleja³², A. Usachov⁸, A. Ustyuzhanin³⁸, U. Uwer¹³,
 A. Vagner⁷⁴, V. Vagnoni¹⁶, A. Valassi⁴³, S. Valat⁴³, G. Valenti¹⁶, R. Vazquez Gomez⁴³,
 P. Vazquez Regueiro⁴², S. Vecchi¹⁷, M. van Veghel²⁸, J.J. Velthuis⁴⁹, M. Veltri^{18,r},
 G. Veneziano⁵⁸, A. Venkateswaran⁶², M. Vernet⁶, M. Veronesi²⁸, N.V. Veronika¹⁴,
 M. Vesterinen⁵⁸, J.V. Viana Barbosa⁴³, D. Vieira⁶⁵, M. Vieites Diaz⁴², H. Viemann⁷⁰,
 X. Vilasis-Cardona^{41,m}, A. Vitkovskiy²⁸, M. Vitti⁵⁰, V. Volkov³⁶, A. Vollhardt⁴⁵,
 D. Vom Bruch⁹, B. Voneki⁴³, A. Vorobyev³⁴, V. Vorobyev^{39,w}, J.A. de Vries²⁸,
 C. Vázquez Sierra²⁸, R. Waldi⁷⁰, J. Walsh²⁵, J. Wang⁴, M. Wang³, Y. Wang⁶⁸, Z. Wang⁴⁵,
 D.R. Ward⁵⁰, H.M. Wark⁵⁵, N.K. Watson⁴⁸, D. Websdale⁵⁶, A. Weiden⁴⁵, C. Weisser⁵⁹,
 M. Whitehead¹⁰, J. Wicht⁵¹, G. Wilkinson⁵⁸, M. Wilkinson⁶², I. Williams⁵⁰, M.R.J. Williams⁵⁷,
 M. Williams⁵⁹, T. Williams⁴⁸, F.F. Wilson⁵², M. Winn⁸, W. Wislicki³², M. Witek³⁰,
 G. Wormser⁸, S.A. Wotton⁵⁰, K. Wyllie⁴³, D. Xiao⁶⁸, Y. Xie⁶⁸, A. Xu³, M. Xu⁶⁸, Q. Xu⁶⁵,
 Z. Xu³, Z. Xu⁵, Z. Yang³, Z. Yang⁶¹, Y. Yao⁶², L.E. Yeomans⁵⁵, H. Yin⁶⁸, J. Yu^{68,aa}, X. Yuan⁶²,
 O. Yushchenko⁴⁰, K.A. Zarebski⁴⁸, M. Zavertyaev^{12,c}, D. Zhang⁶⁸, L. Zhang³, W.C. Zhang^{3,z},
 Y. Zhang⁸, A. Zhelezov¹³, Y. Zheng⁶⁵, X. Zhu³, V. Zhukov^{10,36}, J.B. Zonneveld⁵³, S. Zucchelli¹⁶.

¹Centro Brasileiro de Pesquisas Físicas (CBPF), Rio de Janeiro, Brazil

²Universidade Federal do Rio de Janeiro (UFRJ), Rio de Janeiro, Brazil

³Center for High Energy Physics, Tsinghua University, Beijing, China

⁴Institute Of High Energy Physics (ihep), Beijing, China

⁵Univ. Grenoble Alpes, Univ. Savoie Mont Blanc, CNRS, IN2P3-LAPP, Annecy, France

⁶Clermont Université, Université Blaise Pascal, CNRS/IN2P3, LPC, Clermont-Ferrand, France

⁷Aix Marseille Univ, CNRS/IN2P3, CPPM, Marseille, France

- ⁸*LAL, Univ. Paris-Sud, CNRS/IN2P3, Université Paris-Saclay, Orsay, France*
- ⁹*LPNHE, Sorbonne Université, Paris Diderot Sorbonne Paris Cité, CNRS/IN2P3, Paris, France*
- ¹⁰*I. Physikalisches Institut, RWTH Aachen University, Aachen, Germany*
- ¹¹*Fakultät Physik, Technische Universität Dortmund, Dortmund, Germany*
- ¹²*Max-Planck-Institut für Kernphysik (MPIK), Heidelberg, Germany*
- ¹³*Physikalisches Institut, Ruprecht-Karls-Universität Heidelberg, Heidelberg, Germany*
- ¹⁴*School of Physics, University College Dublin, Dublin, Ireland*
- ¹⁵*INFN Sezione di Bari, Bari, Italy*
- ¹⁶*INFN Sezione di Bologna, Bologna, Italy*
- ¹⁷*INFN Sezione di Ferrara, Ferrara, Italy*
- ¹⁸*INFN Sezione di Firenze, Firenze, Italy*
- ¹⁹*INFN Laboratori Nazionali di Frascati, Frascati, Italy*
- ²⁰*INFN Sezione di Genova, Genova, Italy*
- ²¹*INFN Sezione di Milano-Bicocca, Milano, Italy*
- ²²*INFN Sezione di Milano, Milano, Italy*
- ²³*INFN Sezione di Cagliari, Monserrato, Italy*
- ²⁴*INFN Sezione di Padova, Padova, Italy*
- ²⁵*INFN Sezione di Pisa, Pisa, Italy*
- ²⁶*INFN Sezione di Roma Tor Vergata, Roma, Italy*
- ²⁷*INFN Sezione di Roma La Sapienza, Roma, Italy*
- ²⁸*Nikhef National Institute for Subatomic Physics, Amsterdam, Netherlands*
- ²⁹*Nikhef National Institute for Subatomic Physics and VU University Amsterdam, Amsterdam, Netherlands*
- ³⁰*Henryk Niewodniczanski Institute of Nuclear Physics Polish Academy of Sciences, Kraków, Poland*
- ³¹*AGH - University of Science and Technology, Faculty of Physics and Applied Computer Science, Kraków, Poland*
- ³²*National Center for Nuclear Research (NCBJ), Warsaw, Poland*
- ³³*Horia Hulubei National Institute of Physics and Nuclear Engineering, Bucharest-Magurele, Romania*
- ³⁴*Petersburg Nuclear Physics Institute (PNPI), Gatchina, Russia*
- ³⁵*Institute of Theoretical and Experimental Physics (ITEP), Moscow, Russia*
- ³⁶*Institute of Nuclear Physics, Moscow State University (SINP MSU), Moscow, Russia*
- ³⁷*Institute for Nuclear Research of the Russian Academy of Sciences (INR RAS), Moscow, Russia*
- ³⁸*Yandex School of Data Analysis, Moscow, Russia*
- ³⁹*Budker Institute of Nuclear Physics (SB RAS), Novosibirsk, Russia*
- ⁴⁰*Institute for High Energy Physics (IHEP), Protvino, Russia*
- ⁴¹*ICCUB, Universitat de Barcelona, Barcelona, Spain*
- ⁴²*Instituto Galego de Física de Altas Enerxías (IGFAE), Universidade de Santiago de Compostela, Santiago de Compostela, Spain*
- ⁴³*European Organization for Nuclear Research (CERN), Geneva, Switzerland*
- ⁴⁴*Institute of Physics, Ecole Polytechnique Fédérale de Lausanne (EPFL), Lausanne, Switzerland*
- ⁴⁵*Physik-Institut, Universität Zürich, Zürich, Switzerland*
- ⁴⁶*NSC Kharkiv Institute of Physics and Technology (NSC KIPT), Kharkiv, Ukraine*
- ⁴⁷*Institute for Nuclear Research of the National Academy of Sciences (KINR), Kyiv, Ukraine*
- ⁴⁸*University of Birmingham, Birmingham, United Kingdom*
- ⁴⁹*H.H. Wills Physics Laboratory, University of Bristol, Bristol, United Kingdom*
- ⁵⁰*Cavendish Laboratory, University of Cambridge, Cambridge, United Kingdom*
- ⁵¹*Department of Physics, University of Warwick, Coventry, United Kingdom*
- ⁵²*STFC Rutherford Appleton Laboratory, Didcot, United Kingdom*
- ⁵³*School of Physics and Astronomy, University of Edinburgh, Edinburgh, United Kingdom*
- ⁵⁴*School of Physics and Astronomy, University of Glasgow, Glasgow, United Kingdom*
- ⁵⁵*Oliver Lodge Laboratory, University of Liverpool, Liverpool, United Kingdom*
- ⁵⁶*Imperial College London, London, United Kingdom*
- ⁵⁷*School of Physics and Astronomy, University of Manchester, Manchester, United Kingdom*
- ⁵⁸*Department of Physics, University of Oxford, Oxford, United Kingdom*
- ⁵⁹*Massachusetts Institute of Technology, Cambridge, MA, United States*
- ⁶⁰*University of Cincinnati, Cincinnati, OH, United States*

- ⁶¹*University of Maryland, College Park, MD, United States*
- ⁶²*Syracuse University, Syracuse, NY, United States*
- ⁶³*Laboratory of Mathematical and Subatomic Physics , Constantine, Algeria, associated to ²*
- ⁶⁴*Pontifícia Universidade Católica do Rio de Janeiro (PUC-Rio), Rio de Janeiro, Brazil, associated to ²*
- ⁶⁵*University of Chinese Academy of Sciences, Beijing, China, associated to ³*
- ⁶⁶*South China Normal University, Guangzhou, China, associated to ³*
- ⁶⁷*School of Physics and Technology, Wuhan University, Wuhan, China, associated to ³*
- ⁶⁸*Institute of Particle Physics, Central China Normal University, Wuhan, Hubei, China, associated to ³*
- ⁶⁹*Departamento de Fisica , Universidad Nacional de Colombia, Bogota, Colombia, associated to ⁹*
- ⁷⁰*Institut für Physik, Universität Rostock, Rostock, Germany, associated to ¹³*
- ⁷¹*Van Swinderen Institute, University of Groningen, Groningen, Netherlands, associated to ²⁸*
- ⁷²*National Research Centre Kurchatov Institute, Moscow, Russia, associated to ³⁵*
- ⁷³*National University of Science and Technology “MISIS”, Moscow, Russia, associated to ³⁵*
- ⁷⁴*National Research Tomsk Polytechnic University, Tomsk, Russia, associated to ³⁵*
- ⁷⁵*Instituto de Fisica Corpuscular, Centro Mixto Universidad de Valencia - CSIC, Valencia, Spain, associated to ⁴¹*
- ⁷⁶*University of Michigan, Ann Arbor, United States, associated to ⁶²*
- ⁷⁷*Los Alamos National Laboratory (LANL), Los Alamos, United States, associated to ⁶²*

^a*Universidade Federal do Triângulo Mineiro (UFTM), Uberaba-MG, Brazil*

^b*Laboratoire Leprince-Ringuet, Palaiseau, France*

^c*P.N. Lebedev Physical Institute, Russian Academy of Science (LPI RAS), Moscow, Russia*

^d*Università di Bari, Bari, Italy*

^e*Università di Bologna, Bologna, Italy*

^f*Università di Cagliari, Cagliari, Italy*

^g*Università di Ferrara, Ferrara, Italy*

^h*Università di Genova, Genova, Italy*

ⁱ*Università di Milano Bicocca, Milano, Italy*

^j*Università di Roma Tor Vergata, Roma, Italy*

^k*Università di Roma La Sapienza, Roma, Italy*

^l*AGH - University of Science and Technology, Faculty of Computer Science, Electronics and Telecommunications, Kraków, Poland*

^m*LIFAELS, La Salle, Universitat Ramon Llull, Barcelona, Spain*

ⁿ*Hanoi University of Science, Hanoi, Vietnam*

^o*Università di Padova, Padova, Italy*

^p*Università di Pisa, Pisa, Italy*

^q*Università degli Studi di Milano, Milano, Italy*

^r*Università di Urbino, Urbino, Italy*

^s*Università della Basilicata, Potenza, Italy*

^t*Scuola Normale Superiore, Pisa, Italy*

^u*Università di Modena e Reggio Emilia, Modena, Italy*

^v*MSU - Iligan Institute of Technology (MSU-IIT), Iligan, Philippines*

^w*Novosibirsk State University, Novosibirsk, Russia*

^x*National Research University Higher School of Economics, Moscow, Russia*

^y*Sezione INFN di Trieste, Trieste, Italy*

^z*School of Physics and Information Technology, Shaanxi Normal University (SNNU), Xi'an, China*

^{aa}*Physics and Micro Electronic College, Hunan University, Changsha City, China*

[†]*Deceased*